AN ABSTRACT OF THE THESIS OF

David Trench for the degree of Master of Science in Geology presented on September 4, 2008.

Title: The Termination of the Basin and Range Province into a Clockwise Rotating Region of Transtension and Volcanism, Central Oregon.

Abstract approved:

_____

Andrew J. Meigs

Normal faults characterizing extensional provinces may terminate along-strike at regions of zero extension, at zones of transform faults, or at triple junctions. Termination of the Basin and Range extensional province in southeastern Oregon is thought to occur by right-lateral transform motion distributed across the Brothers Fault zone (BFZ) in central Oregon (Lawrence, 1976). New field mapping across the transition from the Hart Mountain fault, a Basin and Range normal fault, into the BFZ suggests a more complex model for the northern termination of Basin and Range extension. Topographic relief along the Hart Mountain fault decreases to zero approaching the BFZ. Northwest trending BFZ faults simultaneously increase from 5 m of relief to a maximum of 107 m to the northwest away from the zone of transition. Field data indicate that predominantly dip-slip separation with little apparent strike-separation characterize BFZ faults. Independent models of fault slip direction and

style imply, predominantly dip-slip motion for the Hart Mountain faults, oblique slip for the BFZ, and an east-west regional extension direction.

Cross-sections estimate the BFZ has recorded 63 m (± 10 m) of extension, the overlap region between the Basin and Range and the BFZ has recorded 224 m (± 10 m) of extension, and the Hart Mountain system has recorded 157 m (± 10 m) of extension. Faults at the transition between the BFZ and the Basin and Range accumulate extension from both the BFZ and the Hart Mountain system, suggesting a kinematic link between the two. Two episodes of deformation are suggested. Prior to 5.68 Ma, 161 m (± 20 m) of extension accumulated, and an additional 63 (± 20 m) of extension occurred after 5.68 Ma. Cross-section restorations imply the BFZ has slipped independently of the NWBR since 5.68 Ma. Deformation after 5.68 Ma roughly correlates with periods of basaltic magmatism in the BFZ, suggesting a possible link between volcanism and the two-phase extensional history in the study area.

A model for the interaction between the BFZ and the Basin and Range must be compatible with the active deformational field of North America in the Pacific Northwest. Multiple data sets demonstrate that clockwise rotation characterizes the velocity field of the northern Basin and Range extensional province. I propose a model where the BFZ defines a small circle about a pole of rotation in northeastern Oregon, characterized by oblique opening and periodic magmatism, linked to the Basin and Range by horsetail fractures associated with the northward propagating Basin and Range faults. The structural style and temporal development of both the

BFZ and the major Basin and Range faults are forming in response to the clockwise rotation of the Oregon coastal block to the west. This model unites observations from this study area, the active tectonics, and northern Basin and Range magmatism.

The Termination of the Basin and Range Province into a Clockwise Rotating Region of Transtension and Volcanism, Central Oregon.

by
David Trench

A THESIS

submitted to

Oregon State University

in partial fulfillment of
the requirements for the
degree of

Master of Science

Presented September 4, 2008
Commencement June 2009

Master of Science thesis of David Trench presented on September 4, 2008.

APPROVED:

Major Professor, Andrew Meigs

Chair of the Department of Geosciences

Dean of the Graduate School

I understand that my thesis will become part of the permanent collection of Oregon State University libraries. My signature below authorizes release of my thesis to any reader upon request.

David Trench, Author

Acknowledgements

I would like to thank Andrew Meigs for his constant support and encouragement throughout my time at Oregon State University. His critical evaluation of my research and ideas was invaluable in allowing me to complete my manuscript, as were the numerous bike rides he accompanied me on to release pent up stress. A big thank you to Dave Sherrod of the USGS for the insights and company he provided me at the beginning of my field season, getting me off on the right foot and postponing the sheer desolation of southeast Oregon. Many thanks to my graduate committee Anita Grunder, John Dilles, and Yvette Sptiz, your contributions were greatly appreciated. Thanks to the National Science Foundation for providing funding for the project. A great many thanks to all of my family and friends who kept me motivated and pulled me out of my many forays with prolonged procrastination, I never would have finished without you.

TABLE OF CONTENTS

LIST OF FIGURES

LIST OF TABLES

Table Page

Introduction

Normal faults of extensional provinces may terminate along-strike at regions where extensional offset goes to zero, at zones of transform faulting, or at triple junctions (Wernicke, 1992;Faulds & Varga, 1998;Wolfenden et al., 2004). Individual normal faults accumulate maximum displacement near the center of the fault with displacement progressively approaching zero at the tips (King, 1986;Scholz et al., 1993). An extensional province, consisting of many normal faults, may exhibit a decrease in extensional offset at its margin, similar to displacement gradients observed at the tips of individual normal faults (Peacock & Sanderson, 1991;Scholz et al., 1993;Gupta & Scholz, 2000). Additionally, extensional provinces can go to zero extensional offset at volcanic provinces where extension is accommodated by dike injection and magmatism in the crust (Rubin & Pollard, 1988;Rubin, 1992;Rowley, 1998;Tentler, 2005). Transform boundaries terminate extensional provinces where discrete strike-slip faults partition strain between extended and unextended terrains (Burchfiel & Stewart, 1966;Davis & Burchfiel, 1973).

The northwest Basin and Range (NWBR) in southeast Oregon consists of large displacement (>150 m) north-northeast trending normal faults and Basin and Range style extensional topography. The Brothers Fault zone (BFZ) defines the northern boundary of the NWBR separating less extended crust to the north from more extended crust to the south (Fig. 1A) (Lawrence, 1976). The BFZ runs approximately 300 kilometers along a N60ºW trend through central Oregon (Fig. 1B). An interpretation of the BFZ as a strike-slip termination to the Basin and Range is

appealing because the BFZ is approximately parallel to the dominant direction of extension in the NWBR (~ N90ºW) (Pezzopane & Weldon, 1993). Although the NWBR ends at the BFZ, regional topographic trends and fault patterns approaching the BFZ imply a more complex relationship between the BFZ and the NWBR. Previous work (Wernicke, 1992;Faulds & Varga, 1998;Wolfenden et al., 2004) suggests that the NWBR either ends as a diffuse zone of decreasing topographic relief, reflecting the dissipation of slip along many normal faults or ends discretely at a zone of strike-slip of faulting in the BFZ. A third explanation for the termination of the NWBR, is that it links kinematically to the BFZ, where th e BFZ is related to the northward propagation of the NWBR.

To assess the competing kinematic models for the BFZ, field data were collected to catalogue the structural separation of volcanic units along faults and slip approximations of individual faults from piercing points, offset indicators and other criteria. Three cross-sections illustrating regional structural relationships provide estimates of the maximum horizontal extension at the transition between the NWBR and the BFZ and a comparison of the amount of horizontal extension recorded in the NWBR and BFZ south to the north, respectively. Age data from volcanic units and horizontal extension values constrain temporal variations in extension.

Stereographic projections of slip-vectors for the NWBR and BFZ provide constraints on the style of motion expected in the BFZ based on a regional extensional stress regime. Further constraints on the style of motion were provided by regional fault trends and extension directions for the NWBR, which provided estimates of the

ratio of dip-slip motion to strike-slip ratio motion in the BFZ. Placing field data, extension history, and the modeled style of motion in the BFZ, within the active North American deformational field constrains a new model for the kinematic interaction of fault zones at the northwestern margin of the Basin and Range extensional province.

Regional Tectonics

Faulting in central Oregon on the western edge of the NWBR (Fig. 1B) is characterized by NW striking faults of the BFZ and NNE striking faults of the Basin and Range (Donath, 1962;Pezzopane & Weldon, 1993;Crider, 2001). Pezzopane & Weldon (1993) suggested that extension across central Oregon is manifested by a zone of distributed extension and shear, with up to 6 mm/yr of movement. Along the east flank of the Cascade Range, at the western margin of central Oregon, the distributed faulting defining the northern Walker Lane belt dies out approaching Crater Lake and merges into left stepping grabens that project approximately N20ºW into Newberry volcano (Pezzopane & Weldon, 1993). The Walker Lane belt consists of discontinuous right-lateral strike-slip faults that accommodate approximately 15-25% of Pacific-North American plate motion (Wesnousky, 2005). Faults within central Oregon predominantly show normal separation (Lawrence, 1976; Pezzopane & Weldon, 1993) with limited evidence of both right and left-lateral motion. Lawrence (1976) identified four discrete zones of NW trending faults in eastern Oregon that separate blocks broken by normal faulting (Crider, 2001). From north to south the four fault zones are: the Vale, the Brothers, the Eugene-Denio, and the Mount McLoughlin zones. These fault zones are inferred to be Miocene to Holocene in age and are marked by decreasing magnitudes of extension moving north across the four zones. Decreasing extension along Basin and Range faults to the north suggests that the northern two fault zones, especially the BFZ, terminate the NWBR (Lawrence, 1976).

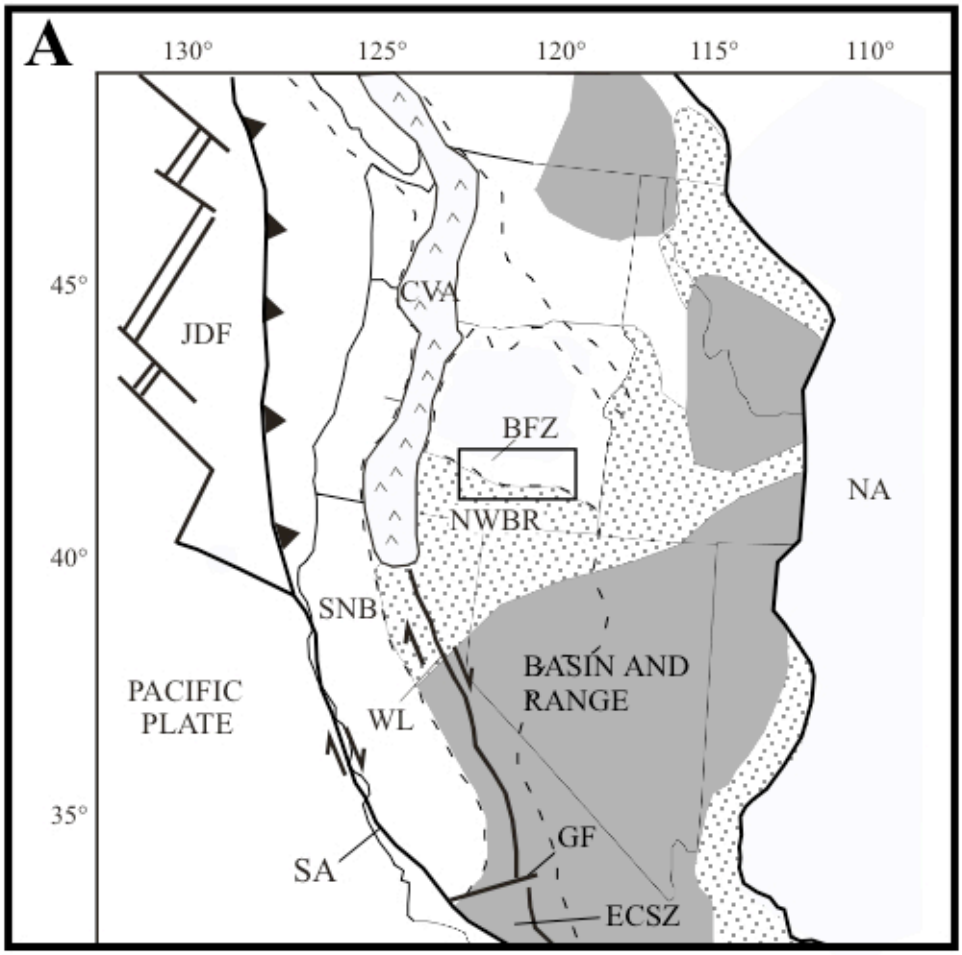

Fig. 1A: Regional tectonic setting of the Brothers Fault zone (BFZ) in central Oregon at the leading edge of the Northwest Basin and Range (NWBR). The light gray and stippled areas represent regions of major (50-100%) and minor (10-20%) Cenozoic extension respectively (Stewart, 1998). The NWBR is located within a broad zone of active deformation (dashed line) and minor extension in Oregon bordered on the west by the Cascade Volcanic arc (CVA) (after Pezzopane & Weldon, 1993). The San Andreas fault (SA) accommodates the majority of motion along the Pacific-North American (NA) plate boundary with distributed fault systems to the west including the Walker Lane belt (WL) accommodating the remaining motion (Wesnousky, 2005). Other major features include the Juan de Fuca plate (JdF), the Garlock fault (GF), and the Eastern California shear zone (ECSZ). Inset box indicates BFZ (**B**). (Modified from Faulds et al., 2005)

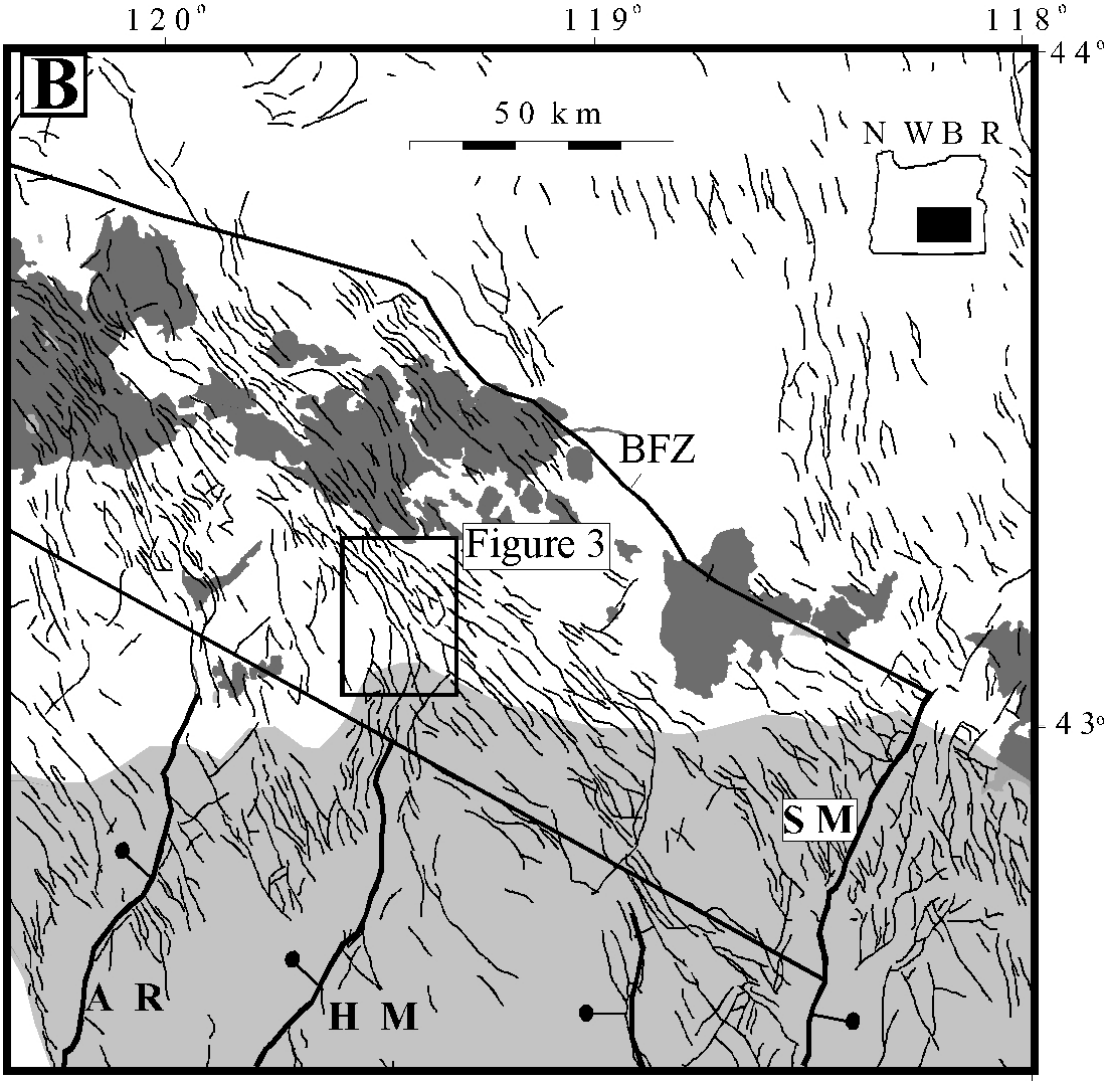

Fig. 1B: Index map of the NWBR shows location of the study area. Distribution of the ~16 Ma Steens flood basalts is in light grey; distribution of Quaternary basalts is in dark shading. Thick lines = large separation (>150 m) regional fault escarpments and thin lines = small separation (<150 m) faults. WR-Winter Ridge; AR-Abert Rim; HM-Hart Mountain (Hart Rim); SM-Steens Mountain (Modified from Jordan et al., 2004).

Brothers fault zone tectonic model

Termination of the Oregon Basin and Range is often compared to the Garlock fault in southern California. Davis & Burchfiel (1973) argued that the Garlock fault originated in response to the large amount of extension to the north of the fault relative to the small magnitude of extension to the south. These observations suggest the Garlock fault is an intracontinental transform fault, which separates extended crust in the north from unextended crust to the south. In evaluating the termination of the Oregon Basin and Range, Lawrence (1976) called upon the Garlock fault as an analog for the BFZ to explain the termination of the NWBR.

The BFZ is characterized by a diffuse system of fault segments that trend approximately N40ºW and range in length from 10 – 20 km. A less abundant population of short, approximately 5 km long, segments trend N30ºW (Lawrence, 1976). Horst and graben topography within the BFZ suggests a component of normal separation in the BFZ (Lawrence, 1976). Based on studies by Tchalenko (1970), Lawrence (1976) concluded that fault patterns in the BFZ as well as the apparent sense of offset within the BFZ mirrored patterns found in other strike-slip shear zones of various scales. Lawrence (1976) further argued that the diffuse population of N40ºW trending en echelon faults represent Reidel shears, within a regional shear zone trending N60ºW across central Oregon. In this model the acute angle between the Reidel shears (BFZ faults; N40ºW) and the overall trend of the shear zone (N60ºW) suggest the fault zone accommodates right lateral motion (Lawrence, 1976). Lawrence (1976) concluded that low slip characterizes the BFZ to explain the absence

of a through-going fault in the BFZ, since through-going fractures are the last to appear within an evolving strike-slip fault system (Tchalenko, 1970).

Right-lateral termination of NWBR extension is a compelling model, but the model does not adequately explain the subtleties of the regional topography, fault trends, the absence of apparent strike-slip motion, or the widespread basaltic volcanism along the BFZ. Crust north of the BFZ shows lesser magnitudes of extension than to the south, but Basin and Range extension does not terminate against the BFZ, instead it shows a gradual decline approaching the fault zone. Furthermore, regional trends indicate mutually cross-cutting relationships between faults of the NWBR and faults of the BFZ that are consistent with a continuous change in fault orientations from the NWBR to the BFZ, as opposed to an abrupt termination of NWBR faults by BFZ faults. A model of the BFZ as a zone of right lateral faults that terminates Basin and Range extension does not account for the gradual decline in topography along Basin and Range structures approaching the BFZ or the smooth change in fault orientations from NNE in the NWBR to NW in the BFZ.

Methods

To assess kinematic nature of the BFZ and its link to the NWBR, field geologic mapping was undertaken at 1:24,000 scale in a region of transition between the NWBR and the BFZ at the northern end of the Hart Mountain fault system. Faults from both the NWBR and the BFZ are clearly expressed topographically within the region. Abundant volcanic units are well dated and span a large range of the late Cenozoic, providing good age constraints on the initiation of faulting and rates of deformation through time. The study area is located approximately 17 miles southeast of Riley, Oregon, west of Harney Basin (Fig. 2).

Geologic mapping focused on the structural relationship between faults and volcanic units, fault and unit locations, structural attitudes on faults and rock units, determination of structural separation and net slip approximations from piercing points, offset contacts and other criteria. Cross-sections were constructed along three profiles through the study area to characterize the magnitude and distribution of extension from south to north through the study area.

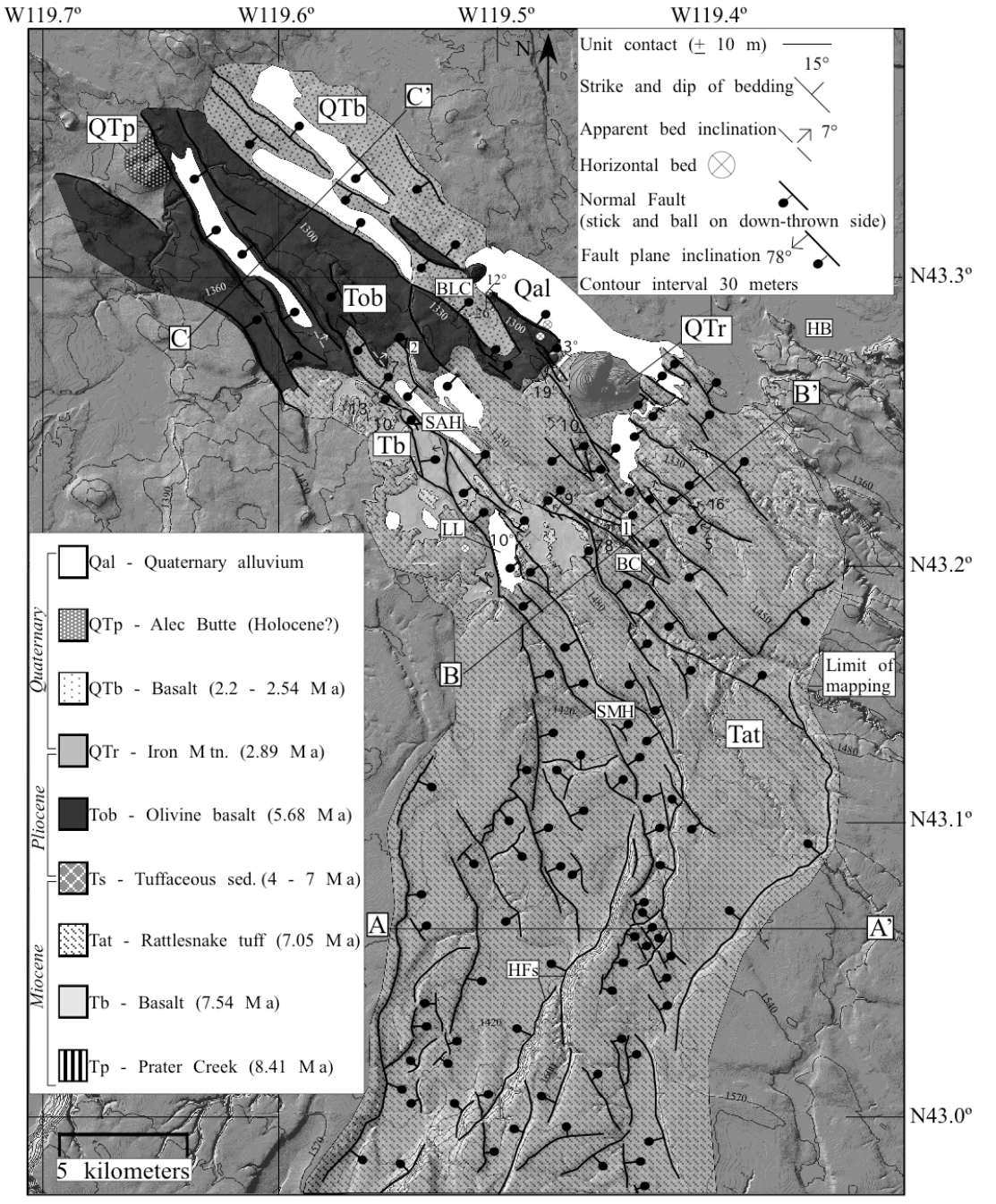

Fig. 2: Geologic map of the study area. AB: Alec Butte; SAH: Sand Hollow; SMH: Smoky Hollow; BC: Buzzard Canyon; BLC: Black Canyon; IRM: Iron Mountain; LL: Lunch Lake; HFS: Hart Mountain fault system. 2: Location of piercing point highlighted in Fig. 6. A-A', B-B', C-C': Denotes locations of cross-sections in Fig. 7. See text for discussion.

Regional stratigraphic succession

Major bedrock units in the study area consist of the Rattlesnake Tuff, a large rhyolite ignimbrite unit, basalt flows of various ages, and isolated volcanic centers. In general, younger units crop out in the north and older units crop out to the south. Miocene and younger rocks have a total exposed thickness of approximately 300m.

The oldest unit in the study area, the 8.41 Ma Prater Creek tuff (Tp) (Jordan et al., 2004), appears at the base of Buzzard Canyon (Fig. 2), as a white crystal–poor, weakly lithified tuff, approximately 12 m thick. There is a second 8 m thick outcrop at the south of end of Lunch Lake. Conformably overlying the small tuff exposure in Buzzard Canyon and at the south end of Lunch Lake, is a 7.54 Ma basalt (Tb) (Jordan et al., 2004), which commonly forms rim rock 4-6 m in thickness. The thickest section is approximately 30 m. The basalt is poorly vesiculated with olivine crystals up to 1 mm and crystals of plagioclase from 0.5mm to 1mm, the crystals are set in a black groundmass with a sugary texture.

The dominant map unit in the study area is the 7.05 Ma Rattlesnake Tuff (Tat), which ranges from 10 to 30 m thick, but can be up to 70 m thick (Streck & Grunder, 1995). The base of the section is whitish gray in color, approximately 1 m thick, with poorly welded pumice clasts up to 5 cm long and lithic clasts of tannish thoeleitic basalt of approximately 4 cm in length. The upper 20 cm of the basal section is partially welded with small pumice clasts of 1-2 cm long and minor elongation. Overlying the basal layer is a thin section (~ 10 cm) of densely welded black vitrophyre. Above the vitrophyre layer, there is a black granular perlitic zone with

granules ranging in size from 5 mm – 1 cm. The upper most section (~ 15 m) of the Rattlesnake, defined as the lithophysal zone (Streck et al., 1999) is devitrified, crystal poor, white to gray in color, with welded, elongated (2 cm – 15 cm) pumice clasts, and flow features and some lithics (~ 2 vol%). Within the study area, the lythophysal section of the Rattlesnake tuff is the dominant outcrop.

Conformably overlying the Rattlesnake tuff throughout most of the study area is a 5.68 Ma microporphyritic basalt (Tob) (Jordan et al., 2004). Small phenocrysts of olivine < 1 mm are set in a black fine grained groundmass (Jordan et al. 2004). Olivine accounts for less than 1 vol% with seriate plagioclase up to 4mm. In one location within the field are there is a greenish brown medium sorted, medium to coarse grain, reworked tuff (Ts) underlying the Tob unit. The reworked tuff contains glass fragments up to 1 mm in size and lithic fragments up to 1 cm with visible bedding structures in the outcrop from 5 mm to 30 cm.

The young, 2.89 Ma (Jordan et al., 2004), Iron Mountain Ryhodacite truncates faults in the northeast corner of the study area (Fig. 2). In a fault bounded valley near Black Canyon (BLC), a younger, 2.2 – 2.54 Ma (Jordan et al., 2004) (QTb) basalt overlyies the Tob unit. The basalt forms rim rock 2-4 m thick and is poorly vesiculated with olivine crystals up to 2 mm and plagioclase crystals up to 1 mm. The crystals are set in a gray to black groundmass with a sugary texture. The Alec Butte basalt at the northwest margin of the study area conformably overlies the Tob unit. The basalt is poorly vesiculated with plagioclase crystals up to 1 mm, set into a black groundmass with sugary texture. Throughout the study area there is a thin cover of

Quaternary alluvium and colluvium on the hill slopes and in the valleys, which obscures both bedrock and fault contacts in many places.

Fault patterns

Faults in the study area include Basin and Range normal faults in the south and BFZ faults to the north (Fig. 2 & 3). The faults are expressed as steep topographic escarpments throughout the study area. Displacement along the faults is inferred from topographic relief and stratigraphic separation. Outcrops are limited to partly eroded footwall exposures, with no observed exposures in the hanging-walls of mapped faults. Topographic relief therefore acts as a proxy for the minimum vertical separation across a fault with the actual dip-slip separation along the faults greater than the observed topographic relief. Neighboring fault segments that exhibit approximately the same topographic relief along strike, within 5 m, are assumed to be linked at depth, even if no fault connects the two segments at the surface (Fig. 4A & B) (Walsh & Watterson, 1991;Trudgill & Cartwright, 1994;Crider & Pollard, 1998;McLeod et al., 2000). Due to colluvium cover throughout the study area and weathering of the basalt units, fault planes were difficult to observe and only one measurement was available. The structural attitude (strike & dip) of rock units is in all cases less than 26º and is restricted to local tilts associated with units draped over fault scarps or units back-tilted towards the faults.

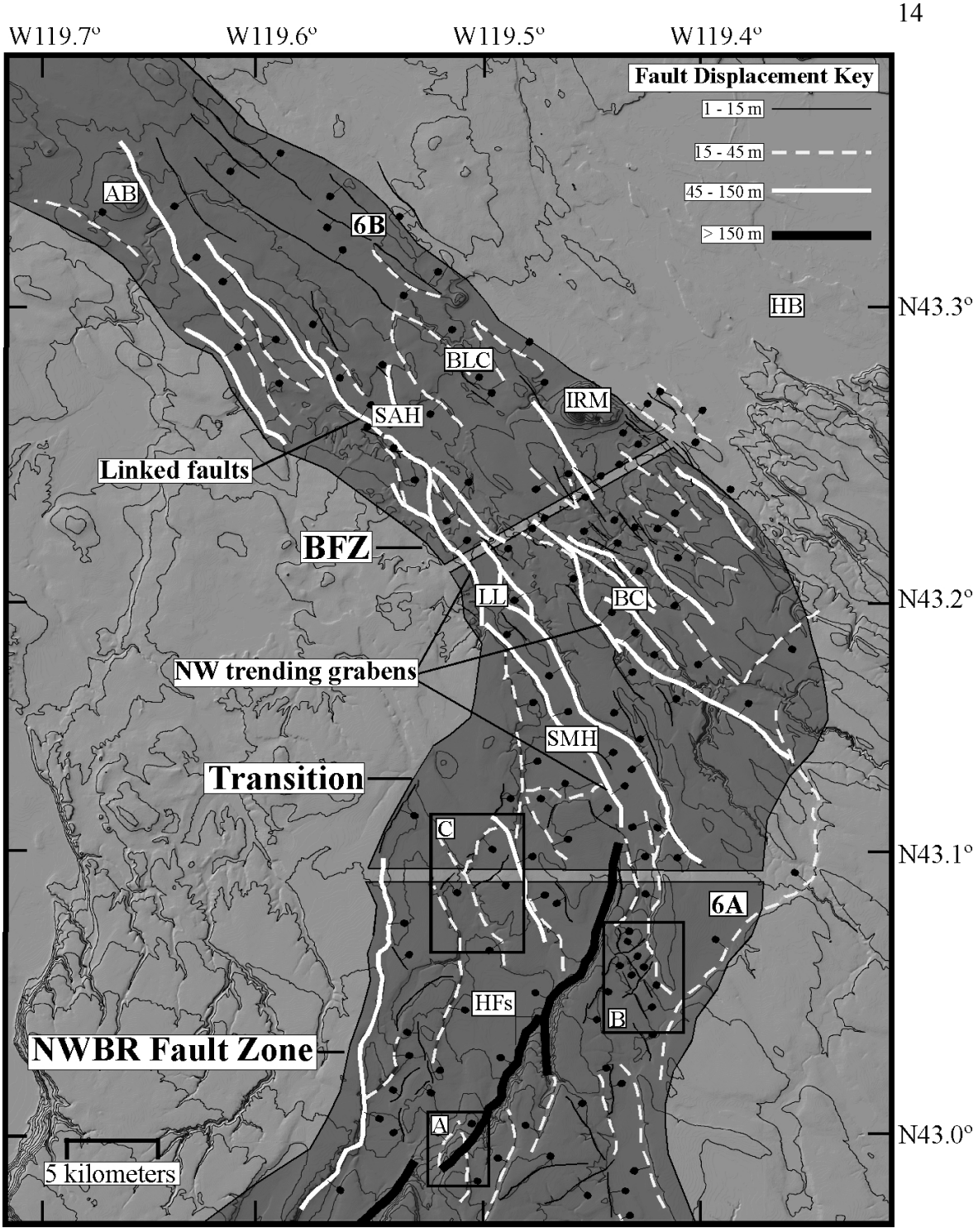

Fig. 3: Weighted fault displacement map based on maximum topographic relief on each fault. Boxes A - C show location of boxes in Figure 5. Large shaded boxes delineate Basin and Range faults, the transition between NWBR faults and BFZ faults, and BFZ faults. Shaded boxes illustrating the NWBR and the BFZ also show fault locations of figure 9A & 9B. See Figure 2 for abbreviation key.

A

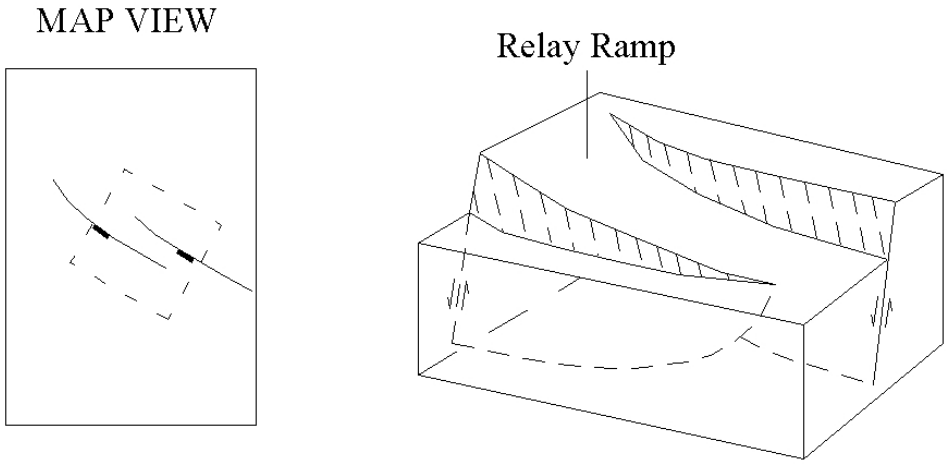

Fig. 4A: Schematic diagram of a fault growth model for linking normal faults in the BFZ. (modified from Crider, 2001).

B

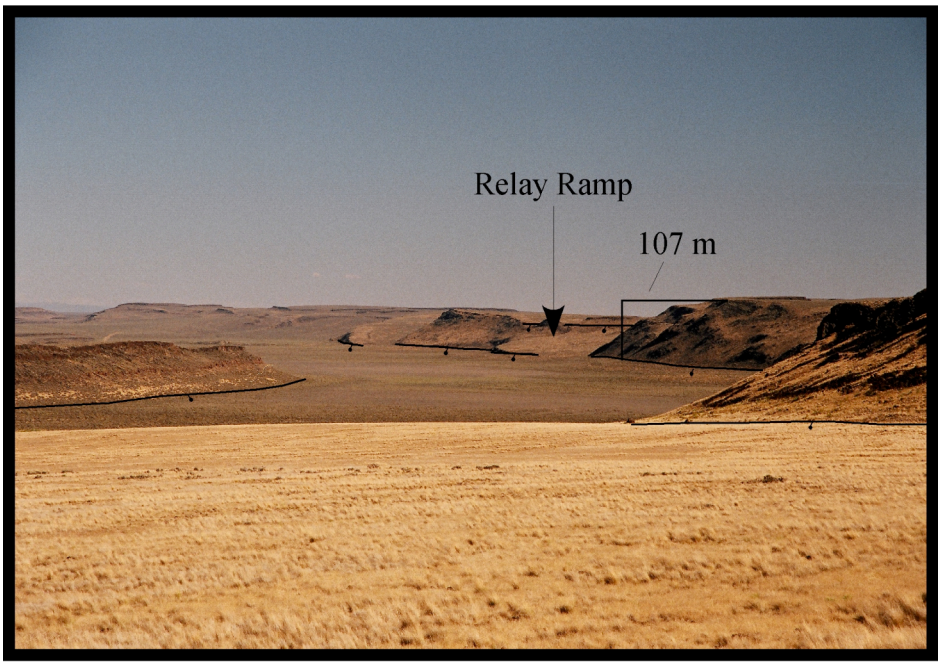

Fig. 4B: Photo looking south along Sand Hollow illustrates a series of linked northeast side down normal faults.

Basin and Range Faults

The Hart Mountain fault system (HFS) is the dominant Basin and Range fault system in the study area (Fig. 3). The northern end of the system extends from the southern margin of the study area along a NNE trend with maximum topographic relief of approximately 155 m. In the study area the HFS consists of two dip-slip fault segments with a total length of 17.6 km linked across the footwall of the southern, shorter fault segment. Shorter NNE trending faults, $\leq$ 14 km, and lesser amounts of topographic relief (60 to 120 m), occur to the west in the hanging-wall and in the footwall of the HFS. A diffuse population of short, (0.5 to 5 km in length) NW trending fault segments appear throughout the southern portion of the study area. Topographic relief on the NW trending fault segments ranges from 5 to 25 m.

Topographic relief decreases on the longer, larger relief faults from south to north. Relief along the HFS system decreases from a maximum of 155 m at the southern end of the study area to zero at the transition between the HFS and the BFZ (Fig. 3). Variations in topographic relief along segments of the short NNE trending faults and the NW trending faults show no systematic south to north decrease in topographic relief as seen along the overall HFS.

Fault patterns in the southern part of the study area illustrate distinct relationships between the longer, large relief, NNE trending faults and the shorter, low relief NW trending faults. Cross-cutting relationships show a NNE trending fault of the HFS cutting a NW trending fault (Fig. 5A). Relationships between the NNE trending fault segments with small offset and faults belonging to the population of

diffuse NW trending faults, indicate a more complex history than cross-cutting relations observed in the HFS. In some areas the NNE trending faults cut the NW trending faults (Fig. 5B), whereas in other locations the NW trending faults truncate NNE trending faults (Fig. 5C). These patterns indicate mutually cross-cutting relationships between the two fault sets. I conclude that NNE trending faults of the HFS predominantly cut NW trending faults to the south and that there is a mutual cross-cutting relationship between the NNE and NW trending segments moving to the north. Fault segments in the southern portion of the study area cut only the 7.05 Ma Rattlesnake Tuff.

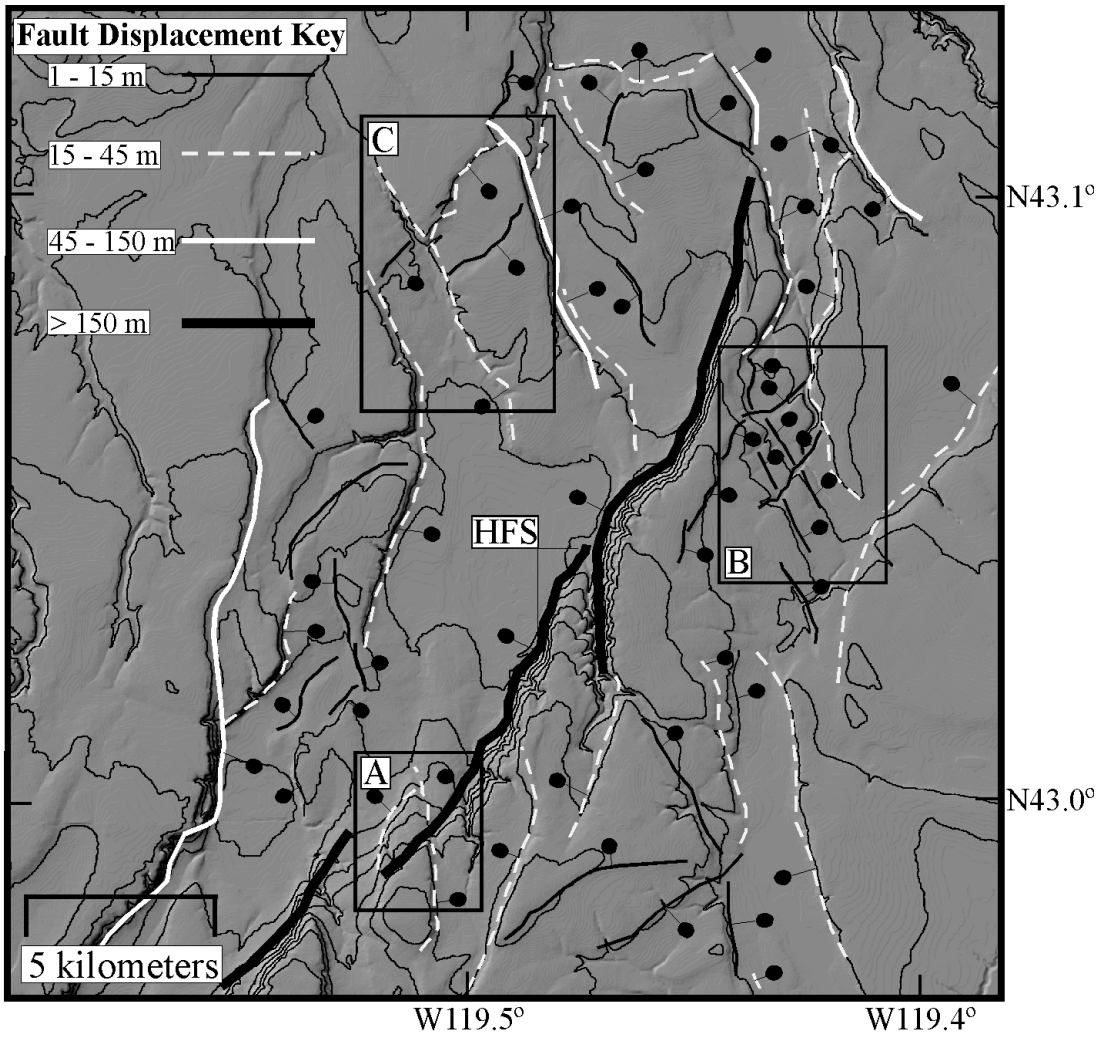

Fig. 5: Boxes A – C illustrate cross-cutting relationships between NNE and NW trending faults. Box A: NNE HFS cuts a NW trending faults. Box B: NNE trending faults cutting NW trending faults. Box C: NW trending faults cutting NNE trending faults.

Transition

The transition between the NWBR and the BFZ faults is marked by an area of low elevation and low topographic relief, with fault orientations changing from NNE trending NWBR faults, to NW trending BFZ faults. North-northeast trending NWBR faults decrease to zero topographic relief at the southern boundary of the transition area. Northwest trending faults of the BFZ increase from 5 m of relief to more than 40 m as the faults continue to the north within the transition area. At the point of intersection between the HFS and the NW trending faults of the BFZ there is a distinct topographic low (Fig. 4). The topographic low between the two systems also marks a continuous change in the dominant fault trend from the NNE trending HFS to the NW trending faults of the BFZ, showing a continuous transition from the Basin and Range into the BFZ. Fault patterns at the region of transition indicate mutually Cross-cutting relationships between NWBR faults and BFZ faults.

Brothers fault zone

The BFZ in the study area is dominated by a series of NW trending grabens bounding Smoky Hollow and Buzzard Canyon and a NW trending NE side down normal fault on the SW side of Sand Hollow (Fig. 4). Fault trends in the BFZ indicate no NNE trending NWBR faults. The Smoky Hollow graben consists of six fault segments ranging in length from 3.4 to 12.4 km, which reach a maximum topographic relief of 90 m at Lunch Lake. Northeast of Smoky Hollow a second fault system defines a NW trending graben along Buzzard Canyon. Buzzard Canyon consists of 4 fault segments ranging in length from 4.3 to 8.1 km, with a maximum topographic

relief of 107 m. A surface fault plane measurement at the northwest end of Buzzard Canyon yielded a strike and dip of N45ºW, 78º NE. This was the only fault plane observed directly.

The escarpments comprising the Smoky Hollow graben system and the Buzzard Canyon system merge into a NW trending escarpment that begins at the north end of Buzzard Canyon and continues to the northwest into Sand Hollow (Fig. 4). This NW trending escarpment consists of six northeast side down normal fault segments ranging in length from 3.3 to 6.2 km. Maximum topographic relief along the escarpment is 107 m at Sand Hollow. At the north end of Sand Hollow topographic relief along the escarpment decreases to zero. As topographic relief decreases along the Sand Hollow escarpment, relief increases from zero to a maximum of 75 m along a series of NW trending grabens to the west of Sand Hollow. This fault system continues to the northwest to Alec Butte (Fig. 4).

A population of NW trending faults appears to the northeast of the main Smoky Hollow and Buzzard Canyon graben systems, with shorter fault segments, less than 4 km, and topographic relief less than 25 m. Although the shorter NW faults are more numerous than the longer NW faults in the study area, they account for less topographic relief than the Smoky Hollow, Buzzard Canyon and Sand Hollow fault systems. Only NW trending faults occur in the northern part of the study area.

BFZ fault motion

Structural relationships with volcanic units in the study area constrain dip-slip and strike-slip separation. A piercing point cut by two NW trending faults for

example, reveals primarily dip-slip separation in the BFZ (Fig. 6A & B). At the north end of Sand Hollow the 5.68 Ma Tob unit goes to zero thickness, which is interpreted as the edge of a paleo-flow. Two escarpments, each showing approximately 5 m of relief at the edge of the flow, subsequently cut the edge of the paleo-flow. Both escarpments show only apparent dip-slip separation with little apparent strike-slip separation. With limited piercing points and no apparent evidence of strike-slip separation in the study area, motion observed at the piercing point along the edge of the Tob unit is taken as a proxy for the style of motion on BFZ faults in the study area.

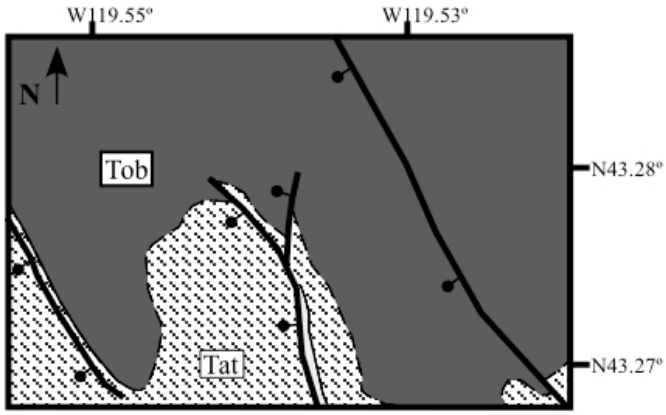

Fig. 6A: Paleo-flow front (dashed line) of a ~5.7 Ma (Tob) basalt pierced by two down to the southeast normal faults. Field mapping of the offset of the paleo-flow front indicates 5 m of dip-slip separation at the tip of the fault with negligible strike-separation.

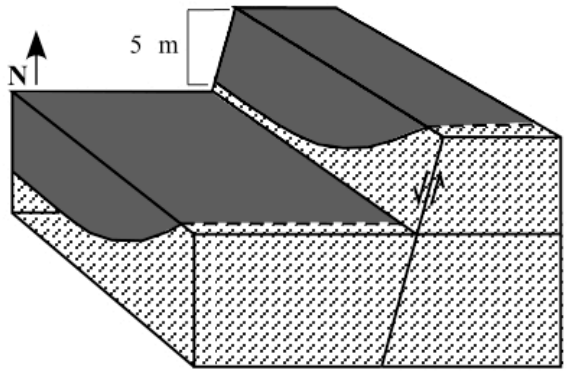

Fig. 6B: Block diagram illustrating dip-slip separation of the flow front, despite apparent strike-separation in map view.

BFZ fault timing

Faults in the BFZ cut progressively younger volcanic units to the north through the study area (Fig. 2). Topographic relief along faults in the study area changes as a function of the age of the unit cut by the faults. Faults in the study area that cut the 7.05 Ma Rattlesnake Tuff, the underlying 7.54 Ma basalt, and the Prater Creek tuff (8.41 Ma) have a maximum relief of 107 m. Faults that cut the younger Tob (5.68 Ma) and Qtb (2.2 – 2.54 Ma) basalt units, have escarpments with a maximum topographic relief of 60 m, with escarpments exhibiting as little as 5 m of relief. The youngest unit in the study area not cut by faults is the 2.89 Ma Iron mountain ryho-dacite (Fig. 2) (Jordan et al., 2004). A series of short NW trending fault segments decrease in topographic relief as they approach Iron mountain in the northeast portion of the study area.

Summary of field observations:

Field observations indicate two discrete fault trends within the study area: NNE trending Basin and Range faults and NW trending BFZ faults. Northwest Basin and Range fault trends indicate both NNE trending and NW trending fault segments, while fault trends in the BFZ indicate only NW trending fault segments. Faults observed within both the NNE trending faults and the NW trending faults indicate predominantly dip-slip separation with no observable strike-separation. Moving from south to north through the study area there is a continuous change from a NNE trend in the south to a NW trend to the north. Cross-cutting relationships illustrate NNE

trending faults predominantly cutting NW trending faults to the south in the Basin and Range. Where the NNE trending HFS and the NW trending BFZ intersect there is a mutually cross-cutting relationship between the two faults set. In the BFZ only NW trending faults occur. Concurrent with the south to north changes in fault orientations is a northward decrease in topographic relief along the HFS. As topographic relief decreases to zero along the NNE trending HFS, relief increases along a series of NW trending grabens at Smoky Hollow and Buzzard Canyon to a maximum of 107 m. To the north in the BFZ basic relief is maintained, but shifts to different fault systems along strike.

Cross-sections

Methods

Three cross-sections were constructed to illustrate the structural style and estimate the amount of extension in the study area (Fig. 7). Separation was measured along three cross-sections by measuring the horizontal and vertical separations along the 7.54 Ma Tb unit in each cross-section. Thickness of the Tb unit is constrained to 30 m through all three cross-sections based on outcrop exposures in Buzzard Canyon. Vertical and horizontal separation on each fault was measured by creating two lines at a 90º angle that connected the interpreted basal contact of the Tb unit in the hanging wall and the footwall. The total horizontal measurements are taken as a minimum extension value across the profiles.

Faults dips for each cross-section are estimated at 75º based on the field measurement at Buzzard Canyon. Horizontal extension in the cross-sections therefore

will vary uniformly as a function of shallower or steeper estimates of fault dips in the study area. A 10º decrease in fault dip results in an approximately two-fold increase in horizontal extension, while a 10º increase in fault dip results in an approximately two-fold decrease in horizontal extension. Measurements of unit thicknesses were difficult to obtain due to limited exposures of basal contacts in the study area. Therefore unit thicknesses are based on previous studies (Streck et al., 1995) and thicknesses as observed in outcrops. Outcrops in the study area do not show significant variations in unit thicknesses and are assumed to be constant along the cross-section lines. Structural tilts in the study area are localized to units draped over fault scarps or back-tilted into footwalls. Based on these observations, units in the cross-sections are predominantly flat-lying, except for an interpreted tilt of approximately 2º in the hanging wall in the HFS. Unit contacts and thicknesses, fault dips, and cross-cutting relationships observed in the study area are projected to depth in the three cross-sections.

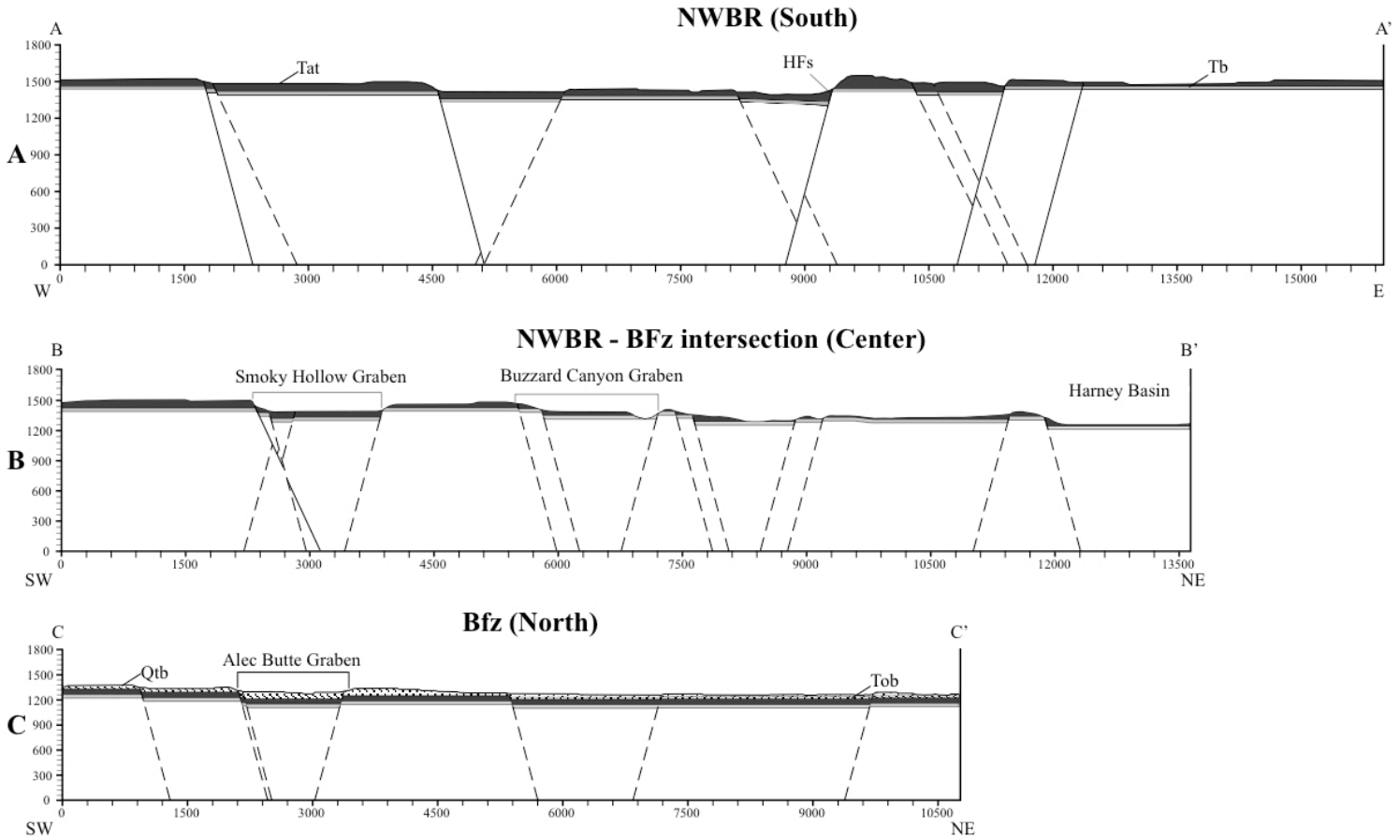

Fig. 7: Cross-sections from south to north through the study area. Faults represented by dashed lines indicate NW trending faults in map view. Faults represented by solid lines indicate NNE trending faults in map view. Unit patterns in the profiles follow map patterns from figure 3. See text for discussion

Regional extension:

The A-A' cross-section traverses the NWBR in the southern portion of the field area, crossing the HFS and small relief (15 - 150 m) NW and NNE trending faults. The HFS accounts for 42 m of horizontal separation and 157 m of vertical separation. Vertical separation measured in the cross-section, 157 m, is larger than the observed topographic relief, 135 m, along the cross-section line, suggesting the topographic relief represents a minimum measurement of vertical separation. The remaining extension is accommodated by lower relief (<150 m) NNE and NW trending faults, with vertical separations measuring from 4 to 96 m and horizontal separations measuring from 2 to 25 m. A total extension value for the A-A' cross-section given the horizontal separation measurements along the individual faults allows for a minimum of 157 m ($\pm$ 10 m) (0.001%) of extension.

The B-B' cross-section crosses the transition between the BFZ and the NWBR. Deformation is primarily accommodated along the NW trending Smoky Hollow graben, and Buzzard Canyon graben in the cross-section (Fig. 7). Vertical separations along the three major faults comprising the Smoky Hollow graben measure 61, 70, and 118 m, from west to east respectively. Horizontal separations measured along those same faults from west to east are 29, 23, and 31 m, respectively. Measurements of the combined vertical separation along the two faults comprising the western rim of the Smoky Hollow graben (131 m) exceed the observed topographic relief of the western rim of the graben, 113 m. Along the eastern rim of the graben the measured vertical separation, 118 m, exceeds the observed topographic relief, 67 m.

Deformation along the Buzzard Canyon graben is similarly localized on three major faults, with vertical separations from west to east of 16, 83, and 48 m, respectively. The corresponding horizontal separation for the three faults is 5, 21, and 13 m. Vertical separation measurements combining the two faults that make up the western rim of the graben (100 m) exceed the observed topographic relief of the western rim of the graben (81 m). In contrast, vertical separation along the eastern rim of the graben, 48 m, is significantly less than the observed topographic relief along the rim, 90 m, which may result from fluvial erosion in the canyon. Deformation along the cross-section ends to the east at Harney Basin, marked by a down to the northeast normal fault with 116 m of vertical separation and 37 m of horizontal separation. The remaining deformation in the cross-section is accommodated along isolated NW trending fault segments with vertical separations ranging from 5 to 25 m and horizontal separations s ranging from 8 to 40 m. Extension across the B-B' cross-section, tabulated from the horizontal separation measurements along individual faults, is 224 m ($\pm$ 10 m) (0.015%) of extension.

The C-C' cross-section captures deformation in the northern portion of the study area across the BFZ. Deformation in the cross-section is primarily accommodated along a NW trending graben that links to the south with the Sand Hollow fault system. The three faults comprising the graben have vertical separations of 62, 17 and 37 m, from west to east respectively, with corresponding horizontal separations of 20, 4, and 10 m, respectively. Vertical separations along western wall of the graben of 62 m and 17 m, are within error of the observed topographic relief

along the fault, 75 m. Isolated NW trending fault segments accommodate the remaining deformation with vertical displacements ranging from 3 to 40 m and horizontal displacements ranging from 1 to 13 m. Extension across the C-C' cross-section, tabulated from the horizontal separation measurements along individual faults, is 63 m ($\pm$ 10 m) (0.005%) of extension.

Cross-section restoration

Methods

Using the extension estimates from the three cross-sections we can restore extension and place spatial and temporal constraints on the distribution of displacement in the study area. Extension recorded in the A-A' cross-section captures NWBR deformation; the B-B' cross-section captures both NWBR and BFZ deformation, and the C-C' cross-section captures deformation in the BFZ. All three cross-sections are linked by at least one of the identified dominant fault systems in the study area. The fault systems are assumed to be linked at depth based on neighboring fault systems exhibiting similar values of topographic relief along-strike ($\pm$ 5 m). The HFS from the A-A' cross-section links to the Smoky Hollow graben in the B-B' cross-section, which links to the Sand Hollow fault system and in turn links to the NW trending grabens approaching Alec Butte in the C-C' cross-section. The distance between neighboring cross-sections and the linkage of at least one dominant fault system between neighboring cross-sections allows for the reasonable assumption that the total offset in one cross-section can be restored fully to the neighboring cross-section.

Using the assumption that neighboring cross-sections are linked and that offset from one cross-section fully restores to the neighboring one, deformation was restored from C-C' to A-A'. For example: the restoration of the C-C' cross-section to an undeformed state would partially restore the neighboring B-B' cross-section with the total extension value from C-C'. Thus the partial restoration of the B-B' cross-section would represent the total extension recorded along the B-B' cross-section minus the extension recorded in the C-C' cross-section. Similarly, the subsequent restoration of the B-B' cross-section to an undeformed state, will partially restore deformation in the A-A' cross-section with the partially restored value of the B-B' cross-section. The partial restoration value of A-A' would therefore represent, the total extension recorded in the A-A' cross-section, minus the partially restored value of the B-B' cross-section.

Ages of the units cut in each cross-section provide temporal constraints on the distribution of deformation. Faults in the northern, C-C' profile, cut the surface of the 2.2 – 2.54 Ma Qtb basalt and the 5.68 Ma Tob basalt (Fig. 2). Therefore extension recorded in the C-C' cross-section captures deformation that occurred after the emplacement of the 5.68 Ma Tob unit. Along the B-B' and A-A' profiles the youngest unit cut is the 7.05 Ma Rattlesnake Tuff (Tat) (Fig. 2). Extension recorded along the two southern profiles, B-B' and A-A', therefore captures deformation after the emplacement the 7.05 Ma Rattlesnake Tuff. Restoration of fault offsets through the study area and unit ages provides a tool to constrain the spatial and temporal

distribution of deformation as well as constrain how the NWBR and BFZ are kinematically linked.

Restored Cross-sections

Starting to the north with the C-C' cross-section, we restore deformation through to the southern part of the study area along the A-A' cross-section. To begin we restore 63 m of extension along the C-C' cross-section since 5.68 Ma, and partially restore the neighboring B-B' profile (224 m). Restoration of 104 m along the C-C' cross-section returns the cross-section to its undeformed state at approximately 6 Ma. Partial restoration of the B-B' cross-section (224 m) with the total extension accumulated in the C-C' cross-section (63 m) implies 161 m of extension on the B-B' cross-section before 5.68 Ma. Within error ($\pm$ 20 m) the partially restored value of the B-B' cross-section (161 m) is equal to extension on the A-A' cross-section (157 m). Thus, the final restoration of the B-B' cross-section (161 m) to a zero value of extension and the partial restoration of the A-A' cross-section (157 m) suggests that, within error ($\pm$ 20 m), no extension accumulated on B-B' and A-A' prior to 7.05 Ma.

The restoration indicates that the A-A' and B-B' cross-sections accumulated 161 m ($\pm$ 20 m) of extension prior to 5.68 Ma, and that the B-B' and C-C' cross-section accumulated 63 m ($\pm$ 20 m) of extension, after 5.68 Ma. Extension recorded in the B-B' cross-section (224 m), equals, within error ($\pm$ 20 m), the sum of the extension recorded in the C-C' cross-section (63 m) and the A-A' cross-section (157 m), which suggests that faults in the B-B' cross-section act as a zone of transition, accumulating extension from NWBR faults to the south (A-A') and BFZ faults to the north (C-C').

Although the B-B' cross-section accumulates extension from both the NWBR to the south (A-A') and the BFZ to the north (C-C'), unequal extension values between the C-C' (63 m) and A-A' (157 m) cross-section suggest that deformation in the NWBR to the south does not fully translate to the BFZ to the north, and vice versa.

To address this question I do a simple thought exercise. If A-A' is restored, what is the partially restored value of B-B'? If C-C' is restored, what is the partially restored value of B-B'? If extension recorded in the NWBR (A-A') fully translates to the BFZ (C-C'), than the partially restored value of the B-B' cross-section should be the same within error ($\pm$ 20 m), regardless of whether B-B' is partially restored with the extension value from the A-A' cross-section or the C-C' cross-section. Partially restored extension values of the B-B' cross-section of 67 m (recovered from A-A') and 161 m (recovered from C-C') indicate that extension recorded along the A-A' cross-section across the NWBR does not transfer to the C-C' cross-section across the BFZ. This suggests that although there is a zone of transition between the BFZ and the NWBR (B-B'), both fault zones have also deformed independently of each other in the last 7.05 Ma.

Timing and rate of deformation

Deformation rates for the study area were determined from the total extension value for a given cross-section divided by the ages of the units cut by faults. Temporal distribution of deformation implies 161 m ($\pm$ 5 m) of extension prior to 5.68 Ma, and 63 m ($\pm$ 5 m) of extension since 5.68 Ma. Faults along the A-A' cross-section accumulated 157 m ($\pm$ 5 m) of extension since 7.05 Ma, resulting in a rate of extension

of 0.02 mm/yr, which is primarily a HFS extension rate. Whereas faults along the C-C' cross-section have accommodated 63 m (± 5 m) of extension since 5.68 Ma, resulting in a deformation rate of 0.01 mm/yr. Restorations suggest the B-B' cross-section accumulated extension from both episodes of deformation before and after 5.68 Ma. Between 5.68 and 7.05 Ma the B-B' cross-section accommodated 161 m (± 5 m) of extension, resulting in a deformation rate of 0.1 mm/yr. After 5.68 Ma, cross-section restorations indicate an additional 63 m (± 5 m) accumulated along the B-B' profile resulting in a deformation rate of 0.01 mm/yr. Extension values and unit ages indicate temporal variations in deformation rates; 0.1 mm/yr prior to 5.68 Ma, and 0.01 mm/yr after 5.68 Ma.

Regional strain direction

Structural relationships between the volcanic units in the study area indicate primarily dip-slip separation. An isolated piercing point in which two BFZ faults pierce the edge of a paleo-flow in the 5.68 Ma Tob unit also illustrate predominantly dip-slip separation with no apparent strike-separation of the paleo-flow front (Fig. 6). Limited field observations of the nature of motion in the BFZ make it difficult to constrain the nature of slip in the fault zone. To complement the field data I use alternative means of slip estimation to place constraints on the nature of slip in the BFZ based on average BFZ fault trends and probable stress directions.

Based on regional fault patterns, an extension direction of 270º to 310º is inferred for the NWBR and the Central Oregon fault zones (Pezzopane & Weldon, 1993). Dip-slip fault motion throughout the NWBR (Christiansen & McKee,

1978;Wernicke, 1992) implies a stress regime favoring extension and therefore a vertical σ_1, based on Coloumb failure criteria (Anderson, 1951), with σ_3 in the horizontal plane of the earths surface, and σ_2 oriented 90º to the least principal stress. A fault dip of 75º is used based on the field measurement at Buzzard Canyon. Using the range of inferred regional extension directions allows for the construction of simple models to constrain the kinematic nature of the BFZ and the NWBR.

BFZ slip vectors

Applying Basin and Range extension directions to the BFZ, provides constraints on whether the faults will slip given the oblique orientation of extension relative to the faults, and predicts potential slip vectors. Studies of regional stress directions in fault populations by Angelier (1979) predict that slip vectors or reactivated fault surfaces can be determined based on the magnitude of the intermediate stress (σ_2) relative to the magnitude of the least principal stress (σ_3) and the maximum principal stress (σ_1). The slip vector on a fault surface parallels the greatest resolved shear stress along that plane (Angelier, 1979). For a given fault orientation there will be multiple stress fields under which existing fractures surfaces will slip, but the slip vector will be contingent on the regional stress field. After the initial failure of a fault surface, the fractured rock will move on an existing plane under a wide range of stress orientations (Davis & Reynolds, 1996). With no cohesive strength to surmount in the rock, movement on the preexisting plane is only inhibited by the frictional resistance to sliding in the fault zone (Davis & Reynolds, 1996).

Models using estimates of 270º and 310º for σ_3 in the NWBR predict slip sense for BFZ and NWBR faults (Fig. 8). Model 1 predicts reactivated slip vectors for the BFZ and the NWBR using a σ_3 of 270º (Table 1.1). Model 2 predicts reactivated slip vectors for the BFZ and the NWBR using a σ_3 of 310º (Table 1). Both Model 1 and Model 2 use an average trend of 324º for BFZ faults and an interpreted fault dip of 75º. Both models have two possible cases of the relative magnitudes of σ_1, σ_2, and σ_3. Case A: $\sigma_1 > \sigma_2 = \sigma_3$; or Case B: $\sigma_1 \geq \sigma_2 > \sigma_3$. In Case A, the slip vector on the reactivated surfaces is predicted by finding the great circle that contains σ_1 and the pole to the average BFZ trend, and the intersection of this great circle with the great circle containing the average BFZ fault trend. In Case B, the slip vector is predicted by finding the great circle that contains σ_3, and the pole to the average BFZ fault trend, and the intersection of the BFZ pole.

Model 1A predicts predominantly dip-slip motion, 056º, 75º (trend and plunge of slip vector), Model 1B predicts greater strike-slip motion, 139º, 18º. In Model 2A, the stereographic projection predicts predominantly dip-slip motion, 056º, 75º, while Model 2B predicts predominantly strike-slip motion, 143º, 03º. Given the relative magnitude of stresses in Case A ($\sigma_1 > \sigma_2 = \sigma_3$), stereographic projections predict predominantly dip-slip motion, 056º, 75º, regardless of extension direction. Similarly, in Case B ($\sigma_1 \geq \sigma_2 > \sigma_3$), stereographic projections predict predominantly strike-slip motion, 139º, 18º and 143º, 03º, regardless of a 270º or 310º extension direction, respectively.

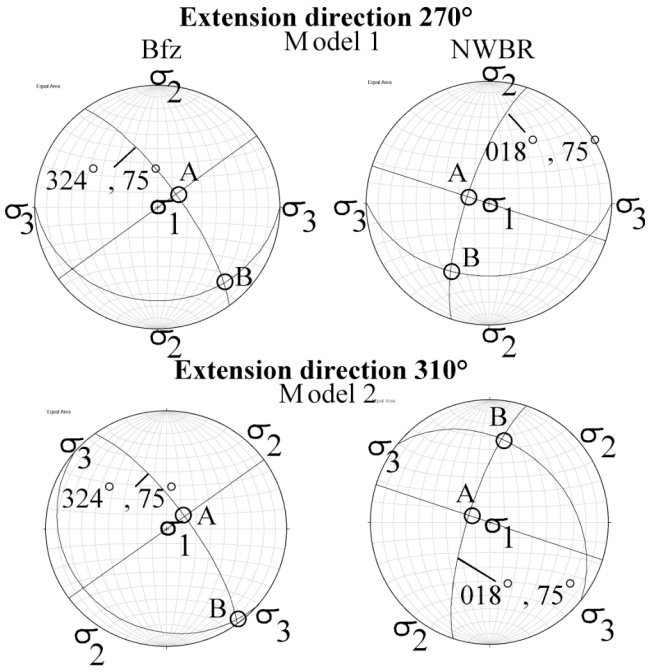

Fig. 8: Lower hemisphere stereonets indicating slip vectors on reactivated fracture surfaces for proposed extension directions in (270° to 310°) the BFZ and NWBR (after Angelier, 1979). For each direction of extension, two reactivated slip vectors are given based on the magnitude of the intermediate stress (σ_2) relative to the greatest principal stress (σ_1) and least principal stress (σ_3). a: Slip vectors on reactivated fracture surfaces if $\sigma_1 > \sigma_2 = \sigma_3$. b: Slip vectors on reactivated fracture surfaces if $\sigma_1 \geq \sigma_2 > \sigma_3$. See text for discussion. (stereonet program courtesy of Rick Allmendinger)

Table 1.1: BFZ slip vectors based on the relative magnitude of σ_1, σ_2, and σ_3 imposed on probable Basin and Range extension directions.

BFZ	**NWBR**
Model 1: σ_3 = 270º (trend and plunge)	Model 1: σ_3 = 270º (trend and plunge)
A: 056º, 75º	A: 285º, 75º
B: 139º, 18º	B: 209º, 36º
Model 2: σ_3 = 310º (trend and plunge)	Model 2: σ_3 = 310º (trend and plunge)
A: 056º, 75º	A: 285º, 75º
B: 143º, 03º	B: 008º, 33º

Performing the same stereographic projections for the NWBR yields similar results to those found in the BFZ (Fig. 8 & Table 1.1). Both projections in the NWBR use an average fault trend of 018º and an average fault dip of 75º. With a 270º extension direction Case A results in predominantly dip-slip motion, 285º, 75º, whereas Case B predicts a greater sense of oblique motion, 209º, 36º. With a 310º

extension direction applied to the average NWBR trend, Case A similarly predicts predominantly dip-slip motion, 285º, 75º, while Case B again predicts a greater sense of oblique motion, 008º, 33º. Models 1 and 2 indicate that in a Case A, where $\sigma_1 \geq \sigma_2 > \sigma_3$, motion in the NWBR will be predominantly dip-slip, 285º, 75º, regardless of the extension direction, while in Case B, where $\sigma_1 > \sigma_2 = \sigma_3$, motion in the NWBR will be more oblique, 209º, 36º and 008º, 33º, respectively.

Discussion of slip vectors

Potential slip-vectors fall into two end-member models, regardless of the extension direction applied to the BFZ: A model of predominantly dip-slip motion and a model of predominantly strike-slip motion. Slip-vectors predicted by the stereographic projections for an average BFZ fault trend, depend largely on the relative magnitude of the principal stresses. Dip-slip motion (056°, 75°) dominates with either a 270° or 310° extension direction, given a stress field in which $\sigma_1 > \sigma_2 = \sigma_3$ (Case A) (Table 1.1). A change in the relative magnitude of the stresses to $\sigma_1 \geq \sigma_2 > \sigma_3$ (Case B), significantly alters the predicted slip-vector to predominantly strike-slip motion (139°, 18° and 143°, 03°) for extension directions of 270° and 310°, respectively (Table 1.1).

Stereographic projections of slip vectors in the NWBR yield similar results to the BFZ, with predominantly dip-slip motion in Case A and a larger component of strike-slip motion in Case B, for both models 1 and 2. Observed motion in the NWBR is predominantly dip-slip (Christiansen & McKee, 1978;Wernicke, 1992;Pezzopane & Weldon, 1993;Crider, 2001), and suggests that the relative magnitude of the principal

stresses in the region is likely similar to the relative stresses found in A, where $\sigma_1 \geq \sigma_2 > \sigma_3$. Using the relative stress magnitudes of the NWBR, $\sigma_1 \geq \sigma_2 > \sigma_3$, as a proxy for the BFZ, we suggest that motion along BFZ faults will be predominantly dip-slip (056º, 75º), despite an oblique orientation to Basin and Range fault trends.

Partitioning of strike-slip and dip-slip motion

The range of extension directions in central Oregon, 270º to 310º, makes predictions of the magnitude of strike-slip and dip-slip motion on the basis of fault trend in the NWBR as well as the BFZ (Table 1.2 & Fig. 9). Average orientations for the two structural domains are 018º for the NWBR and 324º for the BFZ, respectively (Donath, 1962; Lawrence, 1976; Pezzopane & Weldon, 1993). For a NWBR fault with an average trend of 018º, an extension direction of 310º along that trend (Fig. 9A) results in a dip-slip to strike-slip ratio of approximately 2:1 (Table 1.2). An extension direction of 270º along the same 018º NWBR fault trend yields a dip-slip to strike-slip ratio of approximately 3:1 (Table 1.2). Applying extension directions of 310º and 270º to an average BFZ fault trend (Fig. 9B) of 324º results in ratios of dip-slip to strike-slip motion of approximately 0.2:1 and 1:1, respectively (Table 1.2).

Discussion of slip partitioning

The style of faulting in the BFZ is very sensitive to variations in the regional extension direction across central Oregon relative to the NWBR. In Fig. 9B the change in extension direction has a minimal effect on the dip-slip to strike-slip ratio on the NWBR, only changing from 2:1 to 3:1 despite a 40º variation in extension direction. In the BFZ a 310º regional extension direction (Fig. 9B) approximately

parallels the 324º average trend of the fault zone, and as a result, yields a much larger component of strike-slip motion compared to a regional extension direction of 270º. A 40º variation in extension direction along an average BFZ fault trend (324º) results in a five fold change in the dip-slip to strike-slip ratio increasing from 0.2:1 to 1:1, for a 310º and a 270º extension direction, respectively.

Applying the ratios of dip-slip to strike-slip motion for the BFZ to the piercing point identified in the study area (Fig. 9) provides a means to evaluate the field relationships implied by a 270º and a 310º extension direction. A 270º extension direction applied to the piercing point [5 m ($\pm$ 10 m) of topographic relief, i.e. dip-slip motion] implies 5 m of strike-slip motion, while a 310º extension direction implies 25 m of strike-slip motion. Within error ($\pm$ 10 m) the amount of strike-slip motion implied by a 310º extension direction (25 m) should be observable in the field, whereas the strike-slip motion implied by a 270º extension direction (5 m) may not be apparent. The piercing point at the north end of Sand Hollow shows only dip-slip separation, with no apparent strike-slip separation. Furthermore projected slip-vectors in the BFZ (056º, 75º) correlate well with the notion of the BFZ accommodating primarily dip-slip motion. These observations taken with the dip-slip to strike-slip ratios implied by the model suggest a 270º extension is more consistent with field observations than an extension direction of 310º.

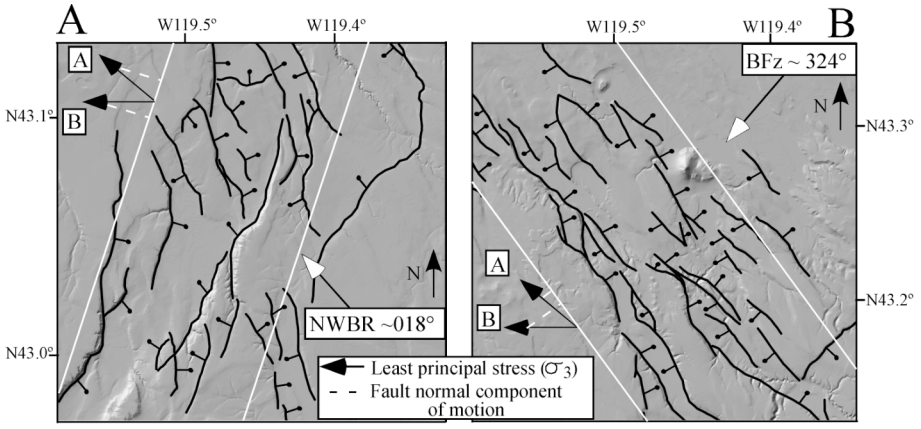

Fig. 9: Implications of variable extension directions (270º to 310º) on the amount of strike-slip and dip-slip motion for faults in the northwest Oregon Basin and Range (Pezzopane & Weldon, 1993). White boxes indicate average trend of the northwest Basin and Range (NWBR) in Fig. 9B and the Brothers Fault zone (BFZ) in Fig. 9B. Black arrows represent range of extension directions (A = 310º, B = 270º; Table 1 & 2).

Table 1.2: Impact of Basin and Range extension direction on the relative distribution of strike-slip and dip-slip motion along BFZ and NWBR faults.

Extension direction	**A:** 310º	**B:** 270º
NWBR (Dip-slip:Strike- slip)	2.3:1	2.7:1
BFZ (Dip-slip:Strike- slip)	.23:1	1.3:1

Regional tectonic models:

The challenge in the BFZ is to understand the coeval growth of two fault systems that intersect at a high angle, have measurable vertical separation, and uncertain amount of strike-separation. Regional fault trends in the NWBR and the BFZ and GPS data suggest two possible kinematic models for the interaction of the NWBR and the BFZ (Fig. 10 & 11).

- The BFZ represents an initial fault fabric formed at the tip of north-propagating Basin and Range normal faults (Fig. 10).
- The BFZ is a small circle transform, formed due to regional rotational deformation about a pole (Fig. 11).

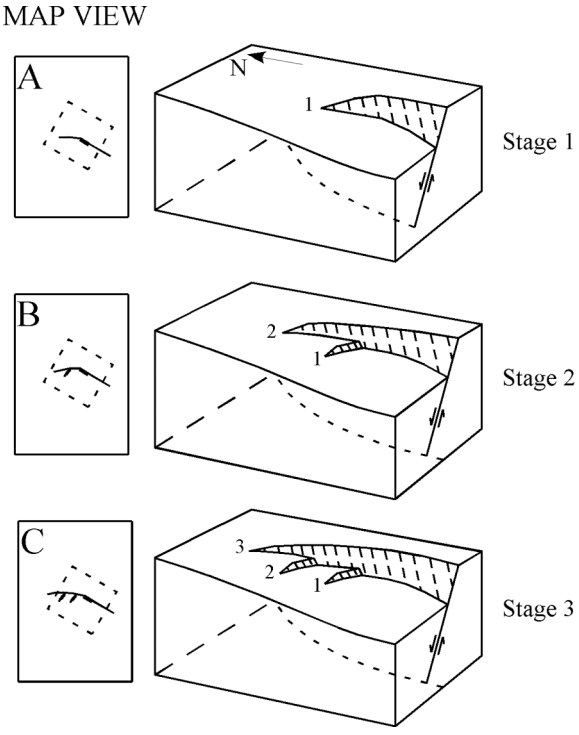

Fig. 10: A: Block diagram of a single normal fault propagating in the hanging wall direction of the fault. B: Block diagram showing a single normal fault propagating along-strike and truncating the initial horsetail propagation. C: Block diagram illustrating continued fault growth and truncation of horsetail fractures (modified from Crider, 2001).

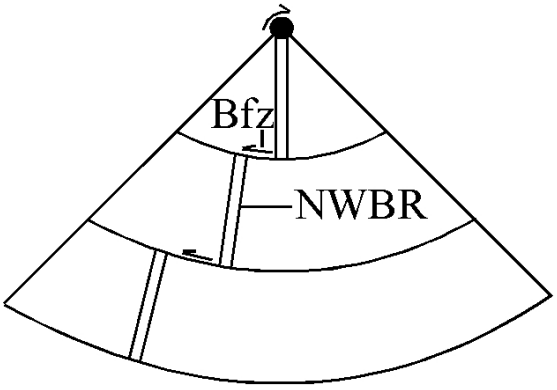

Fig. 11: Simple model of a spreading ridge rotating about a pole.

Central Oregon GPS data:

A variety of data suggest that the Cascadia forearc, or central Oregon block, is moving westward and northward about a pole located in northeast Oregon or eastern Washington (Wells et al., 1998). GPS and paleomagnetic studies (McCaffrey et al., 2000;Wells & Simpson, 2001;Hammond & Thatcher, 2005) have suggested three different Euler poles locations to accommodate the western and northward movement of the central Oregon block and the subsequent extension of central Oregon (Fig. 12). Work by McCaffrey et al. (2000) uses geodetic data to place a best-fit pole for the rotation of the central Oregon block at 45.9º $\pm$ 0.6º N, 241.3º $\pm$ 0.7º E, lying on the Oregon-Washington border. Wells & Simpson (2001) also resolve a pole of rotation for the Oregon coastal block along the Oregon-Washington border at 45.54º N, 119.60º W, but do so from geologic and paleomagnetic data, independent of geodetic data. The two sigma error for the major axis of the Wells & Simpson (2001) pole is 5.1º along a 010º azimuth, with the minor axis at 2.96º. Hammond & Thatcher (2005) meanwhile place the Euler pole for the central Oregon block in northern Oregon, at 44.3º N, 118.04º W.

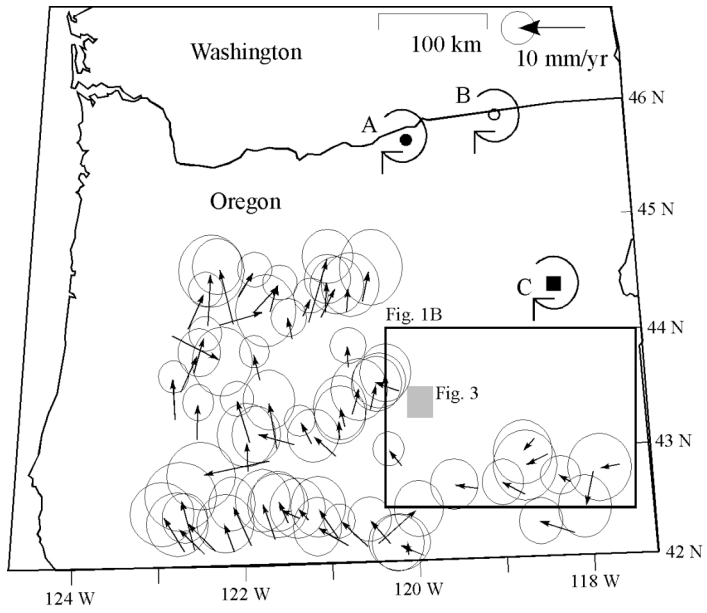

Fig. 12: NWBR GPS velocities (arrows) (Hammond & Thatcher, 2005) with respect to North America (NA). Proposed Euler pole locations for the Oregon coastal block. A: Dark circle: pole defined by Wells & Simpson (2001). B: Open circle: pole defined by McCaffrey et al. (2000). C: Dark box: pole defined by Hammond & Thatcher (2005). Ellipses represent 95 % confidence in GPS velocity with respect to NA (Hammond & Thatcher, 2005) (Modified from McCaffrey et al., 2000).

Propagating normal fault system

Studies of growing strike-slip fault systems indicate that fault tip propagation is preceded by mode I horsetail splay fractures due to displacement loss at the fault tip (Fig. 13) (Granier, 1985;Hancock, 1985;Sylvester, 1988;Bilham & King, 1989;Scholz, 1990;Scholz et al., 1993;Kim et al., 2000). Horsetail fractures therefore record fault tip location and propgation direction (Friedman & Logan, 1970;McGrath & Davison, 1995). As a single fault propagates, the longer fault strand accumulates displacement and progressively cross-cuts the horsetail fractures as the fault increases length (Watterson, 1986;Walsh & Watterson, 1988;Cowie & Scholz, 1992;Dawers & Anders, 1995). In plan view, the growth of a single normal fault will be marked by a gradual change in cross-cutting relationships approaching the propagating tip of the fault (Fig. 11A - C). In earlier formed sections of the fault, the dominant fault will cut the

horsetail fractures. Near the propagating tip of the fault the relationship between the dominant trending fault and the horsetail fractures will be mutually cross-cutting. At the tip of the fault the horsetail fractures branch from the dominant trend of the fault.

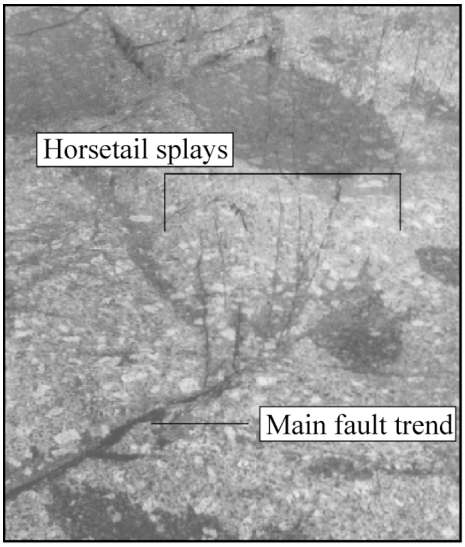

Fig. 13: Photo of a fracture in granite with mode I horsetail splays at the fault tip (scale approximately 2 m) (modified from Scholz, 1991).

Fault patterns within the study area show a continuous transition in fault trends from a NNE trend in the NWBR to a NW trend within the BFZ, with no abrupt alternations between the two fault zones. Similarly cross-cutting relationships indicate a gradual change from a NNE trend in the south to a NW trend in the north (Fig.4). North-northeast trending faults at the southern margin of the study area cut NW trending faults (5A & B). As faults of the NWBR approach the BFZ zone fault relationships are more complex, marked by a transition zone between the two fault sets. Within the zone of transition, NWBR and BFZ faults have mutually cross-cutting relationships, with evidence of NNE trending faults cutting NW trending faults and evidence of NW trending faults cutting NNE trending faults (Fig.5A & B). North of the zone of transition, in the region traditionally defined as the BFZ, NW trending faults dominate (Fig. 4, BFZ).

Fault patterns and cross-cutting relationships within the study area between NNE trending faults of the NWBR and NW trending faults of the BFZ (Fig. 3 & 4) correlate well with regional fault trends in southeast Oregon. Throughout southeast Oregon there is a population of distributed NW trending faults (Fig. 14) surrounding larger displacement (>150 m) NNE trending Basin and Range faults. Recent work in the HLP by Jordan (2005) suggests that the population of NW trending faults throughout south-central Oregon is best viewed as a continuous system, contrary to Lawrence (1976) who suggested the NW trending faults represent discrete zones of strike-slip faulting offsetting major Basin and Range features. Apparent gaps between

fault zones may represent regions where modest topographic offsets are poorly expressed in the younger lavas and sediments (Jordan, 2005).

North-northeast trending faults at Abert Rim, Catlow Rim, and Hart Mountian illustrate a continuous transition from a NNE trend to a NW trend (Fig. 14). Northwest trending faults also have a higher apparent density at the northern termination of the large displacement (>150 m) Basin and Range escarpments. In the region traditionally defined as the BFZ, NW trending faults are the dominant fabric and the major Basin and Range faults no longer apparent (Fig. 14).

Faults of the NWBR do not end abruptly at the BFZ. Rather they lose topographic relief gradually approaching the fault zone. North-northeast trending faults of the NWBR show a clear decrease in relief approaching the BFZ, going to a zero value as the system enters the transition zone at Smoky Hollow. As extension associated with the NWBR decreases to zero topographic relief at the transition zone, extension along BFZ faults increases from 5 m of relief at the intersection between the NWBR and the BFZ to a maximum value of 107 m to the northwest. Displacement profiles of linked faults often display an asymmetric profile versus the bell-shaped profile of a single normal fault, due to low displacement values at the interacting fault tips (Cartwright et al., 1995;Gupta & Scholz, 2000). Similarly, the gradual decrease in relief along NWBR faults into the BFZ and the simultaneous increase in relief along BFZ faults suggests a link between the two systems with displacement transferring from the NWBR to the BFZ.

Cross-section restorations illustrate the kinematic link between the NWBR and the BFZ at the transition between the two fault zones. A maximum of 224 m (± 10 m) of extension occurs at the transition between the NWBR and the BFZ. The extension value at the transition between the two fault sets, 224 m (± 10 m) equals, within error, the sum of the extension in the NWBR and the BFZ, 157 m (± 10 m) and 63 m (± 10 m), respectively. This suggests that where the NWBR and the BFZ overlap in the transition zone, faults accumulate slip from both the NWBR to the south and the BFZ to the north. However, unequal extension values in the NWBR (157 m) and the BFZ (63 m) suggest that the BFZ has a slip history independent of the NWBR, and that NNE trending Basin and Range faults effectively go to zero extension at the BFZ.

The similarities between regional fault patterns and the pattern expected of the along-strike growth of a single normal fault suggests, that fault relationships observed along Abert Rim, Hart Mountain and Catlow Rim may represent the along-strike growth of the NWBR extensional province. Northwest trending BFZ faults at the tips of the large displacement (>150 m) NNE trending faults would represent horsetail fractures at the tip of a single normal fault, propagating along-strike. The continuous transfer of displacement between the NWBR and the BFZ, implied from topographic gradients and cross-section restorations, illustrates that a kinematic link exists between the two fault systems. Fault patterns combined with the implied link between the two fault systems suggests that extension on NNE trending NWBR faults approaches zero at the BFZ, and that the NWBR is propagating into the BFZ.

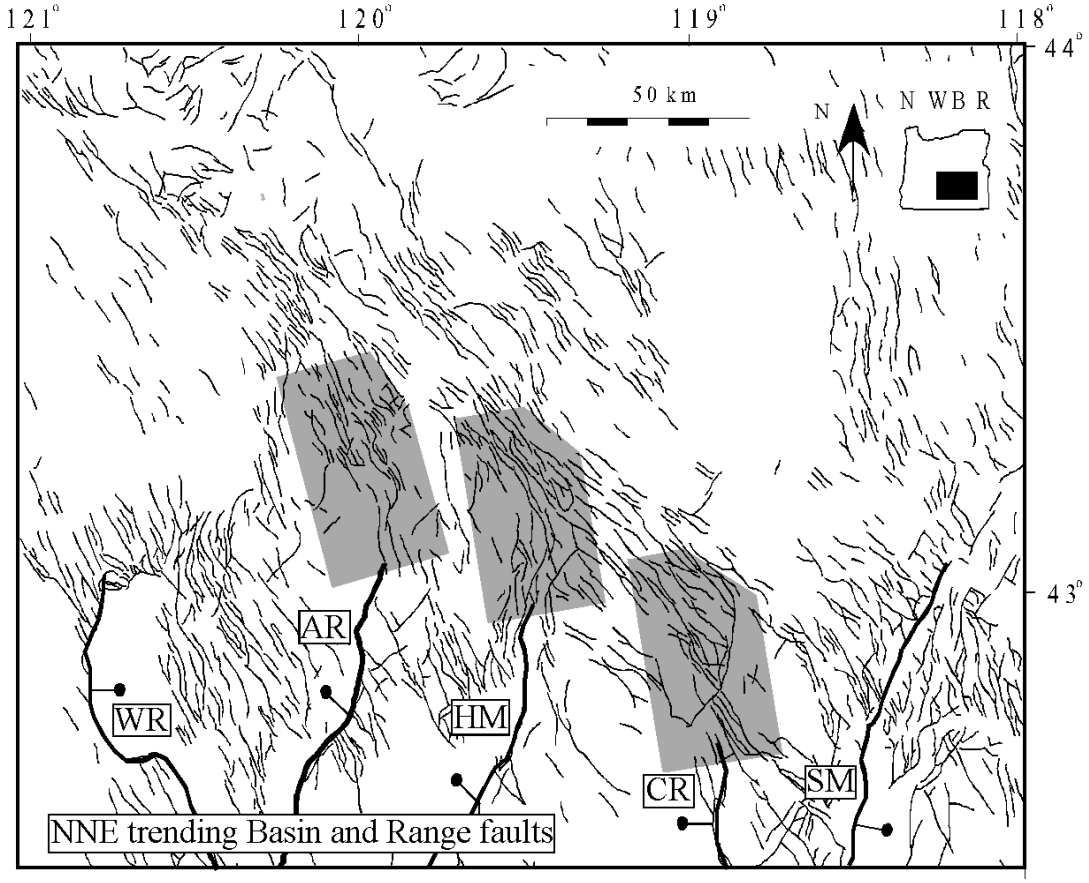

Fig. 14: Regional fault relationships in the NWBR and the BFZ. Shaded boxes indicate possible zones of transition at the tip of large displacement (>150 m) Basin and Range escarpments. Thick lines = large separation (>150 m) regional fault escarpments and thin lines = small separation (<150 m) faults. WR-Winter Ridge; AR-Abert Rim; HM-Hart Mtn.; CR-Catlow Rim; SM-Steens Mtn (Modified from Jordan et al., 2004).

A model of a northward propagating extensional fabric, with the BFZ representing horsetail fractures at the tips of NWBR faults, provides a reasonable explanation of regional fault patterns, cross-cutting relationships, topographic gradients, and the distribution of extension in the NWBR and BFZ. However the model does not adequately explain the independent slip history implied from the cross-section reconstructions. If the BFZ represents a continuation of Basin and Range

extension, than extension recorded in the NWBR should transfer fully to the BFZ. Yet cross-section restorations suggest that although a zone of transition between the two fault systems does accumulate both BFZ and NWBR extension, the BFZ has recorded deformation since 5.68 Ma not apparent in the NWBR. Additionally at the termination of Winter Rim and Steens Mountain the patterns between NNE trending Basin and Range faults and NW trending BFZ faults do not correlate well with the patterns observed along Abert Rim, Hart Mountain and Catlow Rim. At the termination of Abert Rim, Hart Mountain, and Catlow Rim, west-side down normal faults, fault segments transition continuously to the NW in the hanging wall direction of the major Basin and Range faults (Fig. 14). Based on this observation fault patterns at the termination of Winter Rim and Steens Mountain, east-side down normal faults, ought to project to the NE in the hanging wall direction of the fault, yet no NE trending fault segements are observed at the tips of the two Basin and Range faults. The independent slip history observed in the BFZ and the inconsistent fault patterns at the tips of the major Basin and Range faults suggest that although Basin and Range faults may be interacting with BFZ faults, the BFZ does not consist entirely of horsetail splays from the northward propagation of the Basin and Range. Thus a modified framework is necessary to explain kinematic nature of the BF

Brothers fault zone deformation

Regional deformation and cross-section restorations imply a kinematic link between the NWBR and the BFZ, but the cross-section restorations also indicate that the BFZ has a slip history independent of the NWBR. The transition between the BFZ and the NWBR may represent horsetail fractures accumulating slip as a result of Basin and Range extension, but additional mechanisms are necessary to account for the independent slip history in the BFZ since 5.68 Ma. The clockwise rotation of the central Oregon block implied by GPS data and the widespread basaltic volcanism associated with the Oregon High Lava plains (HLP) provide two plausible mechanisms for the independent slip history in the BFZ implied by cross-section restorations.

Clockwise rotation of central Oregon

Implications for the instantaneous velocities and thus the magnitude of extension across the NWBR vary depending on the location of the Euler pole for the central Oregon block. A pole along the Oregon-Washington border implies an instantaneous velocity in the BFZ and the NWBR of approximately 5 mm/yr of westward motion relative to stable North America (NA) (Wells & Simpson 2001, McCaffrey et al 2000). Five mm/yr correlates well with the extension rate of 6 mm/yr estimated by Pezzopane & Weldon (1993) based on geologic deformation in the region. Hammond & Thatcher (2005) suggest an Euler pole in Oregon, which implies an instantaneous velocity of 2 mm/yr of westward motion for the BFZ and the NWBR relative to stable NA. An instantaneous value of 2 mm/yr falls within the uncertainties

of GPS measurements and essentially results in a possible range of 0 – 2 mm/yr for Basin and Range extension in Oregon at a of latitude of 43º N. Extension rates increase clearly to the south towards Nevada (Hammond & Thatcher 2005).

An Euler pole for the central Oregon block in southeast Oregon, or along the Oregon-Washington border, implies a decreasing velocity gradient moving from south to north approaching the pole. Measurements of active deformation in the Basin and Range indicate instantaneous velocities relative to stable NA decreasing from approximately 14 mm/yr near 35º N to approximately 2 mm/yr approaching the NWBR near 41º N (Miller et al., 2001;Bennett et al., 2003). A south-increasing velocity gradient implies concomitantly greater magnitude of extension to the south away from the pole. Kinematically, a clockwise rotation of the central Oregon block and the attendant extension across the province, requires a component of strike-slip motion across central Oregon to accommodate the block rotation and the boundary between less extended crust to the north and extended crust to the south.

Put in the context of a simple model, the NWBR and the BFZ would be analogous to an oceanic spreading ridge and transform opening about an Euler pole (Fig. 11), with the NWBR as the spreading segments and the BFZ as the transform faults. Applying the rotating ridge model to the BFZ and the NWBR would suggest, as does the Lawrence (1976) model, the presence of strike-slip movement along faults in the BFZ. In a model of an oceanic spreading ridge opening about a pole, the magnitude of transform movement increases with distance from the Euler pole in response to the increasing angular velocity. Therefore, the magnitude of transform

motion along the BFZ would be a function of distance from the pole of rotation, rate of rotation, and the duration of extension. Thus, the independent deformation recorded in the BFZ after 5.68 Ma would represent transform motion from the clockwise rotation of central Oregon. This model also suggests that extension would occur north of the BFZ, with the effective end of Basin and Range extension at the pole of rotation. Although this model does provide an explanation the independent slip history in the BFZ, it cannot account for the predominantly dip-slip style of motion observed in the study area and the widespread volcanism in the BFZ.

Magmatic deformation

The BFZ broadly coincides with the High Lava plains province of Oregon. The HLP is a region of late Tertiary to Quaternary bimodal volcanism characterized by widespread basaltic volcanism and northwest age progressive rhyolites (MacLeod et al., 1975;Jordan et al., 2004). Volcanism in the area shows a strong alignment of fissures and vents with the NW trending fault fabric, suggesting lavas have erupted along parallel fissures, which may be structurally controlled. Studies have suggested that the presence of melt localizes deformation in faults and shear zones on a variety of scales and tectonic settings (Rosenberg et al., 2007). Experimental studies indicate that small percentages of melt (< 7 vol%) drastically decrease rock strength (Rosenburg & Handy, 2005).

The widespread intermittent basalt volcanism in the HLP from 10 Ma (Walker & MacLeod, 1991) into the Holocene suggests that melt volumes within the crust have varied time. Three episodes of province-wide basaltic magmatism with possible

periods of heightened activity have been suggested between 7.5 and 7.8 Ma, 5.3 and 5.9 Ma, 2 and 3 Ma (Jordan et al., 2002). Periods of heightened volcanic activity in the province suggested by Jordan et al. (2002, 2004) suggest melt volumes within the crust have varied with time. Because melt volumes within the crust may have varied over time, it is reasonable to suggest that rock strength has varied over time as well. This relationship in which increased melt volumes in the crust decrease rock strength and allow deformation to localize along interconnected melt networks, suggests that deformation in the BFZ might be associated with periods of heightened basaltic magmatism (Jordan et al., 2004;Lawrence, 1976;Rosenberg et al., 2007). Ages of younger basalts (5.68 Ma and 2.2 to 2.54 Ma) in the BFZ indicate a possible correlation with age brackets for periods of heightened magmatic activity in the HLP in the intervals 5.3 and 5.9 Ma and 2 and 3 Ma. Correlating deformation with heightened magmatic activity suggests that the independent slip history in the BFZ after 5.68 Ma may be linked to episodes of heightened magmatic activity between 5.3 and 5.9 Ma and 2 and 3 Ma.

Working model

Expanding from previous regional models, (Christiansen & McKee, 1978; Lawrence, 1976) I propose a model where the NWBR has propagated northward into BFZ within the clockwise rotating central Oregon block. In this model the BFZ acts as a zone of transtension and volcanism, accommodating motion from the clockwise rotation of the central Oregon block and basaltic magmatism associated with the HLP, and linked to the NWBR by horsetail faults at the tips of NNE trending Basin and Range faults.

Episodes of province wide heightened magmatic activity in the HLP between 7.5 and 7.8 Ma, 5.3 and 5.9. Ma and 2 and 3 Ma (Jordan et al., 2004) may have increased melt volumes in the crust and thus decreased rock strength in the HLP crust (Rosenburg et al., 2007). Although there is no structural evidence observed in the study area to establish the initiation of faulting in the BFZ, the episode of heightened activity between 7.5 and 7.8 Ma, which occurred across more than 200 km, may represent the onset of the earliest episodes of deformation in the BFZ (Jordan et al., 2004). A decrease in rock strength coupled with the clockwise rotation of the central Oregon block may have then allowed deformation to localize as small circle transform faults rotating about an Euler pole. The clockwise rotation of the central Oregon block implies transform motion, but field observations and models estimating the sense of slips on BFZ faults suggest that the fault motion is predominantly oblique slip. The absence of any observable strike-slip motion may result from a combination of the proximity of the BFZ to proposed poles of rotation, as well as extensional deformation associated with basaltic magmatism in the HLP.

As the Basin and Range has propagated into Oregon it has created a NW trending fault fabric throughout the region (Fig. 14), associated with the initial horsetail faults at the leading edge of the major range bounding normal faults. Northwest trending horsetail faults at the tips of the major NNE trending NWBR faults subsequently propagated into the BFZ resulting in a kinematic link between the NWBR and the BFZ. This model suggests that NW trending faults of the BFZ have an independent history of transtension associated with the clockwise rotation of the

central Oregon block and HLP basaltic magmatism, as well as a shared history with NNE trending NWBR faults as a result of the propagation of the Basin and Range into Oregon. Therefore the BFZ consists of NW trending faults associated with the rotation of the central Oregon block and HLP magmatism and NW trending horsetail faults related the northward propagation of the Basin and Range. A model of transtension and volcanism provides an updated explanation of the BFZ, suggesting motion in the BFZ results from a combination of magma emplacement, northward growth of the NWBR, and the clockwise rotation of the central Oregon block, versus the extensional origin of right-lateral strike-slip motion suggested by Lawrence (1976).

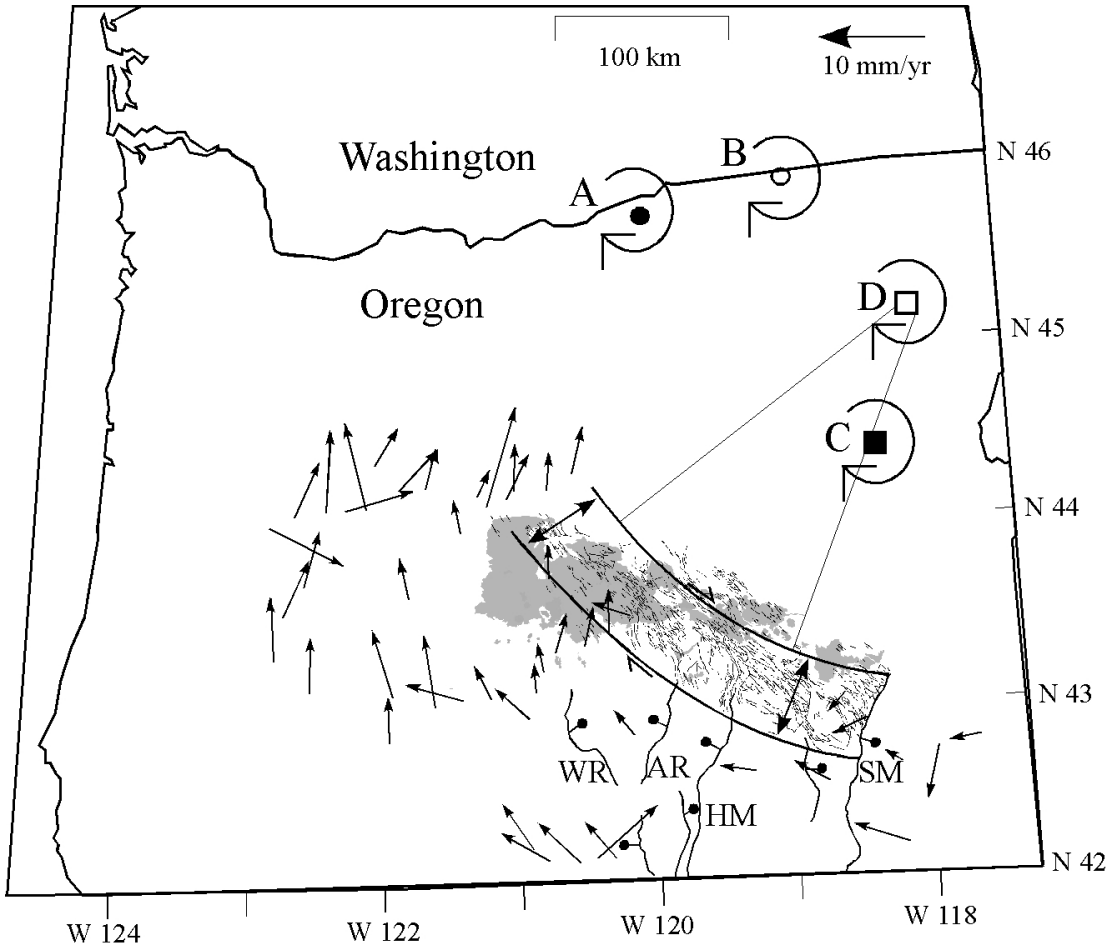

Fig. 15: Working regional tectonic model for the BFZ and the NWBR. Possible Euler pole locations for the central Oregon block. A: Dark circle: pole defined by Wells & Simpson (2001). B: Open circle: pole defined by McCaffrey et al. (2000). C: Dark box: pole defined by Hammond & Thatcher (2005). D: Open box: approximate pole defined by lines tangent to the BFZ envelope. Error ellipses for stations in and immediately south of the BFZ generally equal the signal. Grey shaded area indicates Quaternary basalts. Thick lines = large separation (>150 m) regional fault escarpments and thin lines = small separation (<150 m) faults. WR-Winter Ridge; AR-Abert Rim; HM-Hart Mtn.; SM-Steens Mtn (Jordan et al. 2004, McCaffrey et al. 2000).

Conclusion:

Large displacement (>150 m) NNE trending NWBR faults form the major topography throughout southeast Oregon. Structural relief on NWBR faults decreases from south to north. At the northern end of the Hart Mountain Fault system, topographic relief decreases from a maximum of 155 m to zero at BFZ. The BFZ occurs as a NW trending fabric across central Oregon, with increased fault densities at the tip of NNE trending NWBR faults. The transition between the NWBR and BFZ, is marked by a topographic low, where relief on the NNE trending HFS goes to zero slip while NW trending BFZ faults increase from a minimum of 5 m of relief at the transition between the two fault zones to a maximum of 107 m along principle NW trending graben and linked fault systems. Regional fault patterns illustrate a continuous change in fault trends from NNE trending in the NWBR to NW trending in the BFZ. Similarly, cross-cutting relationships illustrate a change from NNE trending faults that cut NW trending faults, to a zone of mutually cross-cutting faults, to the NW trending faults of the BFZ.

A documented piercing point at the edge of a paleo-flow in the 5.68 Ma Tob unit provides a field constraint on BFZ fault motion indicating predominantly dip-slip separation in the BFZ, with little apparent strike-separation. Stereographic projections of slip vectors, and dip-slip to strike-slip ratios for the BFZ provide further constraints for the style of motion across the BFZ, implying predominantly dip-slip motion despite an oblique orientation to Basin and Range extension.

Horizontal extension measured from cross-sections indicate maximum a value of 224 m at the transition between the NWBR and BFZ, with lesser values recorded in the NWBR (157 m) and the BFZ (63 m). Age data of volcanic units in the study area in addition to cross-section restorations suggest two episodes of deformation, with 157 ($\pm$ 5 m) of extension prior to 5.68 Ma and 63 ($\pm$ 5 m) after 5.68 Ma. Deformation rates implied from horizontal extension values across the three cross-sections suggests 0.1 mm/yr from 7.05 Ma to 5.68 Ma with rates decreasing to 0.01 mm/yr after 5.68.

Cross-section restorations imply a kinematic link between the NWBR and the BFZ, with faults at the transition between the two faults zone accumulating extension from both the NWBR and the BFZ. Although restorations imply a link between the NWBR and the BFZ at the transition between the fault zones, the unequal values of extension in the NWBR and the BFZ, suggest the BFZ has a slip history that is independent of the NWBR. BFZ slip history suggests that deformation after 5.68 Ma (63 m) occurred independently of NWBR extension. The two faults systems are linked, but displacement accumulated on NWBR faults does not fully transfer to BFZ faults.

A joint and independent slip history for the two systems suggests that multiple tectonic forces are acting to cause deformation in the region. Regional fault patterns as well as kinematic relationship between the two fault zones suggest a fault growth model for the NWBR, with the BFZ linked to the NWBR as horsetail fractures at the tips of large displacement (>150 m) NWBR faults. Regional GPS data indicates a

clockwise rotation of the central Oregon block, suggesting a simple spreading ridge model, with the BFZ acting as transform faults offsetting the opening of the NWBR. This model implies increasing magnitudes of strike slip motion along BFZ faults with increasing distance from the pole. The occurrence of widespread volcansim on the BFZ suggests varying crustal melt volumes in time and thus varying rock strength in the region (Rosenberg & Handy, 2005; Rosenberg et al., 2007). No one model adequately describes all of the trends and structure between the NWBR and the BFZ. Therefore I propose a model which combines elements of all three tectonic models, with the BFZ as leaky transform faults at the leading edge of Basin and Range propagation into the clockwise rotating central Oregon block. Although imperfect, this model provides a reasonable kinematic explanation of the nature of the BFZ and its link to the NWBR.

References:

Anderson, E. M. 1951. The dynamics of faulting and dyke formation with applications to Britain. Oliver and Boyd, Edinburgh.

Angelier, J. 1979. Determination of the mean principal direction of stresses or a given fault population. Tectonophysics **56**, T17-T26.

Bennett, R. A., Wernicke, B. P., Niemi, N. A., Friedrich, A. M. & Davis, J. L. 2003. Contemporary strain rates in the northern Basin and Range province from GPS data. Tectonics **22**.

Bilham, R. & King, G. 1989. The morphology of strike-slip faults: examples from the San Andreas Fault, California. Journal of Geophysical Research **94**, 10204-10216.

Burchfiel, B. C. & Stewart, J. H. 1966. The "pull-apart" origin of Death Valley, California. Geological Society of America Bulletin **77**, 439-442.

Cartwright, J. A., Trudgill, B. D. & Mansfield, C. S. 1995. Fault growth by segment linkage: An explanation for scatter in maximum displacement and trace length data from Canyonlands Grabens of SE Utah. Journal of Structural Geology **17**, 1,319-1,326.

Christiansen, R. L. & McKee, E. H. 1978. Late Cenozoic volcanic and tectonic evolution of the Great Basin and Columbia Intermontane regions. Geological Society of America Memoir **152**, 283-311.

Cowie, P. A. & Scholz, C. H. 1992. Growth of faults by accumulation of seismic slip. Journal of Geophysical research **97**, 11,085-11,095.

Crider, J. G. 2001. Oblique slip and the geometry of normal-fault linkage: mechanics and a case study from the Basin and Range in Oregon. Journal of Structural Geology **23**, 1,997-2,009.

Crider, J. G. & Pollard, D. 1998. Fault linkage: Three dimensional mechanical interaction between echelon normal faults. Journal of Geophysical research **103**(B10), 24,373-24,391.

Davis, G. A. & Burchfiel, B. C. 1973. Garlock fault: An intracontinental transform structure, southern California. Geological Society of America Bulletin **84**, 1407-1422.

Davis, G. H. & Reynolds, S. J. 1996. Structural Geology of rock and regions. John Wiley & Sons, Inc., New York.

Dawers, N. H. & Anders, M. H. 1995. Displacement-length scaling and fault linkage. Journal of Structural Geology **17**(5), 607-614.

Donath, F. A. 1962. Analysis of basin-range structure, south-central Oregon. Geological Society of America Bulletin **73**, 1-16.

Faulds, J. E., Henry, C. D. & Hinz, N. H. 2005. Kinematics of the northern Walker Lane: An incipient transform fault along the Pacific-North American plate boundary. Geology **33**(6), 505-508.

Faulds, J. E. & Varga, R. J. 1998. The role of accomodation zones and transfer zones in the regional segmentation of extended terranes. In: Accomodation Zones and Transfer Zones: The Regional Segmentation of the Basin and Range Province (edited by Faulds, J. E. & Stewart, J. H.) **Special Paper 323**. Geological Society of America Boulder, CO.

Friedman, M. & Logan, J. M. 1970. Microscopic feather features. Geological Society of America Bulletin **81**(11), 3417-3420.

Granier, T. 1985. Origin, damping, and pattern of development of faults in granite. Tectonics **4**, 721-737.

Gupta, A. & Scholz, C. H. 2000. A model of normal fault interaction based on observations and theory. Journal of Structural Geology **22**(7), 865-879.

Hammond, W. C. & Thatcher, W. 2005. Northwest Basin and Range tectonic deformation observed

with the Global Positioning System, 1999–2003. Journal of Geophysical Research **110**, B10405.

Hancock, P. L. 1985. Brittle microtectonics: principles and practice. Journal of Structural Geology **7**, 437-457.

Jordan, B. T., Grunder, A. L., Duncan, R. A. & Deino, A. L. 2004. Geochronology of age-progressive volcanism of the Oregon High Lava Plains: Implications for the plume iterpretation of Yellowstone. Journal of Geophysical Research **109**(B10202).

Jordan, B. T., Streck, M. J. & Grunder, A. L. 2002. Bimodal volcanims and tectonism of the High Lava Plains, Oregon. In: Field guide to geologic processes in Cascadia (edited by Moore, G.). Department of Geology and Mineral Industries, Portland, Oregon, 23-46.

Kim, Y. S., Andrews, J. R. & Sanderson, D. 2000. Damage zones around strike-slip fault systems and strike-slip fault evolution, Crackington Haven, southwest England. Geosciences Journal **4**(2), 53-72.

King, G. C. P. 1986. Speculation on the geometry of the initiation and termination process of earthquake rupture and its relation to morphology and geological structure. Pure and Applied Geophysics **124**, 567-585.

McCaffrey, R., Long, M. D., Goldfinger, C., Zwick, P. C., Nabelek, J. L., Johnson, C. K. & Smith, C. 2000. Rotation and plate locking at the southern Cascadia subduction zone. Geophysical Research Letters **27**(19), 3117-3120.

McGrath, A. G. & Davison, I. 1995. Damage zone geometry around fault tips. Journal of Structural Geology **17**(7), 1011-1024.

McLeod, A. E., Dawers, N. H. & Underhill, J. R. 2000. The propagation and linkage of normal faults: insights from Strathspey-Brent-Statfjord fault array, northern North Sea. Basin Research **12**, 263-284.

Miller, M. M., Johnson, D. L., Dixon, T. H. & Dokka, R. K. 2001. Refined kinematics of the eastern California shear zone from GPS. Journal of Geophysical Research **106**(2245-2263).

Peacock, D. & Sanderson, D. 1991. Displacements, segment linkage and relay ramps in normal fault zones. Journal of Structural Geology **13**(6), 721 - 733.

Pezzopane, S. K. & Weldon, R. J. 1993. Tectonic role of active faulting in central Oregon. Tectonics **12**(5), 1,140-1,169.

Rosenberg, C. L., Medvedev, S. & Handy, M. R. 2007. Effects of melting on faulting and continental deformation. In: Tectonic faults: Agents of change on a dynamic earth (edited by Handy, M. R., Hirth, G. & Hovius, N.). The MIT Press, Cambridge, MA.

Rosenburg, C. L. & Handy, M. R. 2005. Experimental deformation of partially melted granite revisited: Implications for the continental crust. Journal of Metamorphic Geology **23**, 19-28.

Rowley, P. D. 1998. Cenozoic transverse zones and igneous belts in the Great Basin, western United States: Their tectonic and economic implications. In: Accomodation zones and Transfer Zones: The Regional Segmentation of the Basin and Range Province (edited by Faulds, J. E. & Stewart, J. P.) **Special Paper** Geological Society of America Boulder, Colorado.

Rubin, A. M. 1992. Dike-induced faulting and graben subsidence in volcanic rift zones. Journal of Geophysical Research **97**(B2), 1839-1858.

Rubin, A. M. & Pollard, D. D. 1988. Dike-induced faulting in rift zones of Iceland and Afar. Geology **16**, 413-417.

Scholz, C. H. 1990. The mechanics of earthquakes and faulting. Cambridge University Press, Cambridge, United Kingdom.

Scholz, C. H., Dawers, N. H., Anders, M. H. & Cowie, P. A. 1993. Fault growth and fault scaling laws: Preliminary results. Journal of Geophysical research **98**, 21,951-21,961.

Stewart, J. H. 1998. Regional characteristics, tilt domains, and extensional history of the late Cenozoic Basin and Range province, western North America. In: Accomodation zones and Transfer zones: The Regional Segmentation of the Basin and Range Province (edited by Faulds, J. E. & Stewart, J. H.) **Special Paper 323**. Geological Society of America, Boulder, Colorado.

Streck, M. J. & Grunder, A. L. 1995. Crystallization and weldiing variations in a widespread ignimbrite sheet; the Rattlesnake Tuff, eastern Oregon, USA. Bulletin of Volcanology **57**, 151-169.

Streck, M. J., Johnson, J. A. & Grunder, A. L. 1999. Filed guide to the geology of the Rattlesnake Tuff and High Lava Plains, eartern Oregon. Oregon Geology **61**(3), 64-76.

Sylvester, A. G. 1988. Strike-slip faults. Geological Society of America Bulletin **100**, 1666-1703.

Tentler, T. 2005. Propagation of brittle failure triggered by magma in Iceland. Tectonophysics **406**, 17-38.

Trudgill, B. & Cartwright, J. 1994. Relay-ramp forms and normal fault linkages, Canyonlands National Park, Utah. Geological Society of America Bulletin **106**, 1143-1157.

Walker, G. W. & MacLeod, N. S. 1991. Geologic Map of Oregon. U.S. Geological Survey, Denver.

Walsh, J. J. & Watterson, J. 1988. Analysis of the relationship between displacement and dimensions of faults. Journal of Structural Geology **10**, 239-247.

Walsh, J. J. & Watterson, J. 1991. Geometric and kinematic coherence and scale effects in normal fault systems. In: The geometry of normal faults (edited by Yielding, A. M. & Freeman, G.) **Special Publication**. Geological Society of London, London, 193-206.

Watterson, J. 1986. Fault dimensions, displacement, and growth. Pure and Applied Geophysics **124**, 365-373.

Wells, R. E. & Simpson, R. W. 2001. Northward migration of the Cascadia forearc in the northwestern U.S. and

implications for subduction deformation. Earth Planets Space **53**, 275-283.

Wells, R. E., Weaver, C. S. & Blakely, R. J. 1998. Fore arc migration in Cascadia and its neotectonic significance. Geology **26**, 759-762.

Wernicke, B. 1992. Cenozoic extensional tectonics of the U.S. Cordillera. In: The Cordilleran Orogen: Conterminous U.S. (edited by Burchfiel, B. C., Lipman, P. W. & Zoback, M. L.) **The Geology of North America**. Geological Society of America, Boulder, CO.

Wesnousky, S. G. 2005. Active faulting in the Walker Lane. Tectonics **24**, 35.

Wolfenden, E., Ebinger, C., Gezahegn, Y., Deino, A. & Dereje, A. 2004. Evolution of the northern Main Ethiopian rift: birth of a triple junction. Earth and Planetary Science Letters **224**(1-2), 213-228.

APPENDIX

APPENDIX A: Unit Descriptions

Prater Creek tuff (8.41 Ma) (Tp): White crystal poor, weakly lithified tuff, lithics up to 1 cm, approximately 12 m thick.

Tb (7.54 Ma): Poorly vesiculated basalt with olivine crystals up to 1 mm and crystals of plagioclase from .5mm to 1mm. Crystals set in a black groundmass with a sugary texture. Generally appears as rimrock 4-6m.

Rattlesnake Tuff (7.05 Ma) (Tat): Base of the section (~1m), poorly welded, pumice clasts 5-7cm, lithics of tholeitic basalt ~ 4cm tannish in color. Upper 20cm partially welded with small pumice clasts 1-2cm and minor elongation. Thin section (~ 10cm) of black vitrophyre about partially welded section. Above the vitrophyre layer, there is a black granular perlitic zone with granules ranging in size from 5mm – 1cm. Upper most section lithophysal zone (~ 120m), devitrified, crystal poor, white to gray in color, welded pumice clasts, elongated 2cm – 15cm, with flow features and some lithics ~ 2%.

Tob (5.68 Ma): Microporphyritic basalt, small phenocrysts of olivine < 1mm in a black fine grained groundmass. Olivine less than < 1%. Seriate plagioclase up to 4mm.

Ts (4 – 7 Ma): Greenish brown medium sorted , medium to coarse grain reworked tuff. Glass fragments 1mm and lithics up to 1cm. Visible bedding structures, with bedding from 5mm to 30cm.

Iron Mountain (2.89 Ma) (QTr): Light gray rhyodacite, crystal poor, highly vesiculated.

QTb (2.2 – 2.54 Ma): Poorly vesiculated basalt with olivine crystals up to 2mm and plagioclase crystals up to 1mm. Crystals set in a gray to black groundmass with a sugary texture. Generally appears as rim rock 2-4m

Alec Butte (Holocene?) (QTp): Poorly vesiculated basalt with plagioclase crystals up to 1 mm, set in a black groundmass with a sugary texture.

Q: Alluvium and lake deposits

APPENDIX B: Geologic map of the study area

W119.7º W119.6º W119.5º W119.4º

N43.3º

N43.2º

N43.1º

N43.0º